

## 1 **Supplementary Information**

2 Reconciling the total carbon budget for boreal forest wildfire emissions using airborne observations

3  
4 Katherine L. Hayden<sup>1\*</sup>, Shao-Meng Li<sup>2</sup>, John Liggio<sup>1</sup>, Michael J. Wheeler<sup>1</sup>, Jeremy J.B. Wentzell<sup>1</sup>, Amy  
5 Leithead<sup>1</sup>, Peter Brickell<sup>1</sup>, Richard L. Mittermeier<sup>1</sup>, Zachary Oldham<sup>1,6</sup>, Cris Mihele<sup>1</sup>, Ralf M. Staebler<sup>1</sup>,  
6 Samar G. Moussa<sup>1</sup>, Andrea Darlington<sup>1</sup>, Mengistu Wolde<sup>3</sup>, Daniel Thompson<sup>4</sup>, Jack Chen<sup>1</sup>, Debora  
7 Griffin<sup>1</sup>, Ellen Eckert<sup>1</sup>, Jenna C. Ditto<sup>5</sup>, Megan He<sup>5</sup> and Drew R. Gentner<sup>5</sup>

8 [1]{Air Quality Research Division, Environment Canada, Toronto, ON, Canada}

9 [2]{College of Environmental Sciences and Engineering, Peking University, Beijing, China}

10 [3]{National Research Council of Canada, Ottawa, ON, Canada}

11 [4]{Canadian Forest Service, Natural Resources Canada, Edmonton, ON, Canada}

12 [5]{Yale University, New Haven, CT, USA}

13 [6]{University of Waterloo, Waterloo, ON, Canada}

14  
15 \*Correspondence to: Katherine Hayden (katherine.hayden@ec.gc.ca)

## 17 **12.0 Methods**

### 18 **12.1 Aircraft measurements**

19 Table S1 provides a summary of the measurements with associated instrumentation, technical details and  
20 related references.

#### 21 **12.1.1 Trace gas measurements**

22 All of the trace gas instrumentation except NH<sub>3</sub> and the CIMS were sampled through PTFE tubing from a  
23 main aircraft roof hatch that contained multiple inlet ports through which rear-facing tubing was mounted.

24 **The rear-facing inlet minimizes the sampling of particles.**

25 **NO, NO<sub>2</sub>, NO<sub>y</sub>, SO<sub>2</sub> and GEM** ~~These measurements were made using modified commercial instruments~~

26 ~~(Thermo Scientific Inc. and Tekran Instruments Corp.)~~—NO and SO<sub>2</sub> were directly measured: NO by

27 chemiluminescence with excess ozone using a 42i TL instrument operated in single mode, while SO<sub>2</sub> was  
28 measured by pulsed fluorescence with a 43i TL instrument. A photolytic converter (Air Quality Design  
29 Inc.) was used to selectively convert a large fraction of NO<sub>2</sub> to NO. The sum of this NO<sub>2</sub> fraction that  
30 was converted to NO plus ambient NO, defined as NO<sub>c</sub>, was measured by a second 42i TL  
31 chemiluminescent instrument and then NO<sub>2</sub> was calculated based on NO<sub>c</sub>, NO and the efficiency of the  
32 photolytic converter. NO<sub>y</sub> was measured by using an external molybdenum converter heated at 325 °C  
33 and placed as close as possible to the sampling point, followed by a third 42i TL instrument. NO and SO<sub>2</sub>  
34 calibrations were conducted by generating mixing ratios of 0-100 ppbv using NIST certified cylinders  
35 from Scott-Marin (10.3 ppmv accuracy: +/- 2 %), an Environics (Model 6100 Multi-Gas Calibrator), and  
36 a Sabio Zero Generator (Model 1001). The efficiencies of the photolytic and NO<sub>y</sub> converters were  
37 determined using the gas phase titration option of the Environics calibrator. ~~Gas phase elemental Hg~~  
38 ~~(GEM) was measured with a Tekran 237X instrument (Tekran Instruments Corporation) modified to~~  
39 ~~allow a reduced sampling time of 2 min (McLagan et al., 2021; Cole et al., 2014).~~ Calibrations were  
40 conducted periodically throughout the measurement study using NIST-certified standards. Instrument  
41 zeros were performed for these instruments 3-5 times per flight for a duration of ~3-5 minutes each time  
42 at the beginning, during and after each flight.

43 ~~NH<sub>3</sub> Ammonia (NH<sub>3</sub>) measurements were conducted using Los Gatos Research's (LGR's) NH<sub>3</sub>/H<sub>2</sub>S~~  
44 ~~Analyzer (Model 911-0039) was~~ sampled through an unfiltered inlet, critical orifice and 4 m of 6.35 mm  
45 (1/4") outer diameter Sulfinert-coated tubing heated to 90 °C to minimize NH<sub>3</sub> losses to the tubing walls.  
46 The flow rate was 2.5 LPM, controlled through a critical orifice near the unfiltered inlet with the pressure  
47 in the fluoropel-coated LGR cell being maintained at 100 Torr. For instrument zeros, ambient air was  
48 passed through a Teflon filter coated with citric acid. Calibrations were performed using a certified  
49 ammonia standard (Air Liquide; 10.0 ppm NH<sub>3</sub> in N<sub>2</sub>, accuracy: +/- 5 %), diluted to near-ambient levels.

50 ~~CO, CO<sub>2</sub>, CH<sub>4</sub>, TC and NMOG<sub>f</sub>~~ CO, CO<sub>2</sub>, CH<sub>4</sub> were measured with a Cavity Ring Down (CRD)  
51 spectroscopy instrument (Picarro G2401-m).

52 **TC and NMOG<sub>T</sub>** A second Picarro G2401-m instrument was used to measure total carbon (TC, in units  
53 of ppmv C) by passing the sample air through a heated (650 °C) platinum catalyst (Shimadzu), adapted  
54 from Stockwell et al. (2018) and Veres et al., (2010) which converted all carbon species to CO<sub>2</sub>.  
55 Approximately 4 g of platinum catalyst  
56 ([https://www.elementalmicroanalysis.com/product\\_details.php?product=B1605&description=High%20Sensitivity%20Catalyst%20630-00996](https://www.elementalmicroanalysis.com/product_details.php?product=B1605&description=High%20Sensitivity%20Catalyst%20630-00996)) was enclosed in a resistively heated ½” O.D. x 12” long stainless  
57 steel tube. As the catalyst assembly was mounted on the roof exterior to the aircraft, with no unheated  
58 portion of inlet, TC losses were expected to be negligible. NMOG<sub>T</sub> mixing ratios in units of ppmv C ~~was~~  
59 ~~were~~ quantified by subtracting the ambient CH<sub>4</sub>, CO and CO<sub>2</sub> measurements (instrument without the  
60 ~~upstream~~-catalyst) from the TC measurements (Fig. S2). Calibrations using two different mixing ratio  
61 standards of CO, CO<sub>2</sub> and CH<sub>4</sub>, traceable to NOAA GMD standards,- were performed for both Picarro  
62 instruments during flight (at the beginning and end) ~~of each flight~~ to assess instrument drift and  
63 sensitivity. No significant drift was observed during each flight. NMOG<sub>T</sub> was averaged to 10 sec (from  
64 the 2 sec native time resolution) to increase the signal to noise ratio. The uncertainty of each instrument  
65 was assessed in flight by overflowing the inlet with a constant flow of calibration gas or an ultra pure  
66 nitrogen gas stripped of CO<sub>2</sub> via two NaOH pellet traps in series  
67 (<https://www.sigmaaldrich.com/CA/en/product/supelco/503215>). In both cases, this resulted in an  
68 uncertainty of approximately 60 ppbv C at the 3σ level for each TC channel (dominated by the precision  
69 of the CO<sub>2</sub> measurement) (Fig. S2). These uncertainties were added in quadrature resulting in a 3σ  
70 uncertainty of ±85 ppb C for NMOG<sub>T</sub>. Laboratory experiments indicated that the conversion efficiency  
71 of ethane across the catalyst was ~100 %, which is expected to be the most challenging species to  
72 combust aside from methane, which is concurrently measured. Additional laboratory experiments using a  
73 range of hydrocarbons (>C<sub>2</sub>) including aromatics also exhibited ~100 % conversion efficiency (Li et al.,  
74 2021; Li et al., 2019). The catalyst material was changed after approximately every 5 flights to further  
75 ensure minimal changes in efficiency.  
76

77 **CIMS** The CIMS (~~modified Tofwerk/Aerodyne Api-ToF~~) instrument sampled from an insulated rear-  
78 facing inlet (PFA, 3/8" OD, 1/4" ID) at 7 LPM (0°C, 1 atm). The instrument was operated using iodide as  
79 a reagent ion. The mass resolution at an internal standard peak ( $^{13}\text{CC}_2\text{H}_6\text{O}_2\text{I}^-$ ) was ~5400 Th/Th. The  
80 reagent ion was generated by passing 2 sLpm (0°C, 1 atm) of UHP  $\text{N}_2$  over a methyl iodide permeation  
81 tube held at 40 °C. This flow was then passed through a Polonium-210 ionizer (NRD P-2031) into the  
82 ion molecule reactor (IMR). A flow of humidified  $\text{N}_2$  (20 sccm through a stainless steel bubbler) was  
83 also added to the IMR in order to keep the ratio of  $\text{I}(\text{H}_2\text{O})/\text{I}^-$  as constant as possible. The IMR and small  
84 segmented quadrupoles (SSQ) were pressure controlled to 70 and 1.5 mBar respectively using Alicat  
85 pressure controllers (PC-EXTSEN). Instrument zeros were performed every 15 min by flooding the inlet  
86 with 10 sLpm (0°C, 1 atm) of air that had been passed through a Pt/Pd catalyst (CD Nova) heated to  
87 350 °C followed by bicarbonate and charcoal scrubbers (United Filtration). A flow (50 sccm) of  
88 isotopically labelled propanoic acid ( $^{13}\text{CC}_2\text{H}_6\text{O}_2$ ) was constantly added to the inlet during the campaign to  
89 track instrument sensitivity. Compounds were identified using known/expected sensitivities and available  
90 calibration standards (Tables S3).

91 **PTRMS** The PTR-ToF-MS (~~Ionicon Analytik GmbH, Austria~~) used chemical ionization with  $\text{H}_3\text{O}^+$  as  
92 ~~the primary reagent ion was operated~~ in a configuration described previously (Table S1). Gases with a  
93 proton affinity greater than that of water were protonated in the drift tube. The pressure and temperature  
94 of the drift tube region were maintained at a constant 2.15 mbar and 60 °C, respectively for an E/N of 141  
95 Td. The unit contained a catalytic converter heated to 350 °C with a continuous flow of ambient air at a  
96 flow rate of one litre per minute. A permeation tube with 1,2,4-trichlorobenzene was placed at the inlet to  
97 improve the ~~sensitivity-accuracy~~ of the mass calibration for higher masses. Instrumental backgrounds  
98 were performed in flight using a custom-built zero-air generating unit. The data were processed using  
99 Tofware software (Tofwerk AG). Calibrations were performed on the ground using gas standard  
100 mixtures from Ionicon, Apel-Reimer and Scott-Marrin for 20 compounds (Table S3). ~~For compounds~~  
101 ~~with no available gas standard, a relative response factor was calculated with reaction rate constants using~~  
102 ~~the method described in Sekimoto et al. (2017) and guided by the work of Koss et al. (2018) to define an~~

103 ~~additional 169 ions.~~ Compound identifications for molecular formulas for the PTRMS and CIMS data  
104 were assigned based on a limited set of possibilities (particularly for the smaller compounds), known or  
105 expected compound sensitivities, and previously published laboratory work by Koss et al. (2018); this is  
106 more fully described in the SI Sect. 2.1.3.

107 **AWAS** The Advanced Whole Air Sampler (AWAS) was used to ~~take 20-30 sec integrated 'grab' collect~~  
108 ~~ambient~~ samples using 1.33-litre electropolished stainless steel canisters in rack-mounted arrays of 12-  
109 canister modules (Lerner et al., 2017, and references therein). A metal bellows compressor (Senior  
110 Aerospace Metal Bellows, MB-158) was used to pressurize canisters to approximately 30 PSI over a  
111 period of approximately ~~15 sec (30 sec maximum)~~ 20 to 30 sec. Sample lines and manifold tubing were  
112 continually flushed with ambient air during the flights. Sampling took place by activating module and  
113 pump system valving with custom Labview-based software operating a data logger interface (Labjack  
114 Corp., Model T7). The samples were analysed ~~between 5 and 9 days after the flight and cleaned as soon~~  
115 ~~as possible after the flight~~ with an analytical system installed at the Fort McMurray International Airport.  
116 The on-site analytical system consisted of a custom fabricated gas chromatograph (GC) system using  
117 cryogenic sample pre-concentration, 2-dimensional gas chromatography, Mass Spectrometric Detection  
118 (MS) and Flame Ionization Detection (FID). Sample air was cryogenically trapped at -185 °C on a glass  
119 bead-filled trap, thus condensing/solidifying the hydrocarbons, and subsequently thermally desorbing  
120 them at 135 °C into the multi-column, multi-oven GC/MS/FID instrument. Trapped sample air volumes  
121 were calculated by recording pressure differences in a volume-calibrated downstream vacuum vessel  
122 before and after sample trapping. Duplicate analysis was carried out on one canister in each AWAS  
123 module. The analytical separation of approximately 120 chemical species was carried out by use of a pre-  
124 column (SPB-1) where the initial separation of compounds according to boiling point occurred. The low  
125 molecular weight compounds (C<sub>2</sub> to C<sub>4</sub>) were then directed to two RTX-QS columns connected in series  
126 and quantified by a FID. The higher molecular weight compound stream (C<sub>4</sub> to C<sub>10</sub>) was subsequently  
127 split and simultaneously analysed by a second FID connected to an Aluminum Oxide/KCL column (C<sub>4</sub> to  
128 C<sub>8</sub>) and by a quadrupole Mass Spectrometer (Agilent Technologies, 5977B) connected to an HP-1 column

129 by means of a fused silica tubing restrictor (C<sub>7</sub> to C<sub>10</sub>). The precolumn and RTX-QS columns were  
130 mounted in the main oven of the gas chromatograph (Agilent Technologies 7890B) and thus were subject  
131 to one temperature program. The AlO<sub>x</sub>/KCL and HP-1 analytical columns were each mounted in a  
132 separate temperature-controlled GC oven module (Agilent Technologies, LTM Series II) and operated  
133 with a different temperature program. Detector peak areas were calibrated with primary gas standard  
134 mixtures in the ppbv concentration range obtained from Apel-Reimer Environmental Inc. (U.S.A.) and  
135 the National Physical Laboratory (UK). Compound retention time drift and potential detector sensitivity  
136 changes were monitored and compensated for by means of daily analysis of a secondary standard gas.  
137 The AWAS modules were cleaned by a custom-fabricated, automated cleaning system similar to that of  
138 Lerner et al. (2017). ~~Toluene, benzene and xylenes were not quantified because the method and  
139 columns used were not optimized for these compounds. Analytical issues due to incomplete water vapour  
140 management in the sample gas stream resulted in retention time shifts and some peak broadening effects  
141 resulting in elevated uncertainties. Uncertainties are estimated at ±25 % for C<sub>2</sub> to C<sub>5</sub> and C<sub>6</sub> alkanes  
142 detected by FID, and ±40 % for C<sub>6</sub> alkenes, and the C<sub>7</sub> to C<sub>10</sub> species detected by MS.~~

143 **Cartridges** Integrated gas phase samples were collected using an automated adsorbent tube sampling  
144 assembly (i.e. cartridge) that was mounted in an under-wing pod (see Ditto et al., 2021; ~~SI Sect. 2.1.1~~).  
145 ~~Adsorbent tubes were packed with quartz wool, glass beads, Tenax TA, and Carboxen 100 (or “QBTX”),~~  
146 ~~similar to those discussed in Sheu et al. (2018). Samples were collected over the lower set of aircraft~~  
147 ~~transects and higher set of transects, resulting in two integrated cartridge samples for each screen; only~~  
148 ~~the lower altitude samples are used in the analysis as the samples for the higher set of transects included a~~  
149 ~~transect that was above the wildfire plume.~~ Samples were shipped to Yale University where offline  
150 analysis was conducted using thermal desorption (GERSTEL TD 3.5+) followed by gas chromatography  
151 (Agilent 7890B), atmospheric pressure chemical ionization, and high-resolution mass spectrometry  
152 (Agilent 6550) to speciate gas-phase organic compounds (Ditto et al., 2021, Sheu et al., 2018, Khare et  
153 al., 2019). ~~The samples provided targeted measurements of gas phase compounds ranging in volatility~~  
154 ~~from C<sub>10</sub> volatile organic compounds (VOCs) to C<sub>25</sub> semivolatile organic compounds (SVOCs) including~~

155 ~~hydrocarbons (CH) as well as functionalized compounds containing 1 oxygen atom (CHO<sub>1</sub>), and 1 sulfur~~  
156 ~~atom (CHS<sub>1</sub>).~~ Ion abundances for CH, CHO<sub>1</sub>, and CHS<sub>1</sub> species were converted to mass concentrations  
157 assuming average response factors that were calculated based on calibrations using the NIST Reference  
158 Gulf of Mexico 2779 Macondo Crude oil reference material following Khare et al. (2019), which  
159 accounts for variations in response and fragmentation between components of the complex mixture.  
160 CHN<sub>1</sub> species were not quantitatively converted to mass due to the lack of comprehensive and available  
161 authentic standards. ~~We acknowledge the limited sample numbers based on flight design, and that t~~The  
162 reported emissions are subject to potential variations in sampling efficiency within the under-wing  
163 sampling pod across C<sub>10</sub>-C<sub>25</sub> and, in the event of losses due to analyte breakthrough, would likely be  
164 considered lower limit estimates. ~~Prior b~~Breakthrough testing with QBTX adsorbent tubes and similar  
165 sampling conditions to those used in this study showed that analyte trapping efficiency in the same carbon  
166 number range was generally greater than 85 % (Sheu et al., 2018). ~~CHN<sub>1</sub> was not quantitatively~~  
167 ~~converted to mass due to the lack of available standards.~~ For CH, CHO<sub>1</sub>, and CHS<sub>1</sub>, each group of  
168 isomers at a given carbon number was categorized by molecular formula, according to their double bond  
169 equivalents (DBE) ranging from 0 to 15. Emission ratios (to in-plume CO) were estimated for CH, CHO<sub>1</sub>  
170 and CHS<sub>1</sub> using observed concentrations for the C<sub>10</sub>-C<sub>25</sub> species summed across DBEs. Further  
171 discussion of these methods can be found in Ditto et al. (2021), including in the SI (i.e., Section S3).

## 172 **12.1.2 Particle measurements**

173 Particles were sampled from a forward-facing isokinetic stainless steel diffuser inlet (Droplet  
174 Measurement Technologies) that was positioned near the top of the fuselage forward of the engine on the  
175 starboard side. Theoretical calculations that take into account the inlet dimensions, volume flow and  
176 velocity indicated a 97 % transmission efficiency for particles < 1 μm through the inlet. Air was pulled  
177 through the inlet into a main 0.5" O.D. stainless steel sampling line maintained at the isokinetic rate of 70  
178 LPM by two venturis mounted on the fuselage in the aft section of the aircraft. The aerosol instruments  
179 subsampled from the main sampling line.

180 **AMS** The high resolution aerosol mass spectrometer (AMS) (Aerodyne) measures submicron particles  
181 that are sampled through a critical orifice and focussed through an aerodynamic lens into a region of low  
182 vacuum. The particles impact a heated surface (600 °C), are vapourized and ionized by 70eV impaction.  
183 Ions are then transferred to a time-of-flight mass spectrometer (Tofwerk) where they are accelerated by  
184 electric fields and separated by their velocities which are dependent on their mass to charge ratios. Ions  
185 are then detected by charged microchannel plates. The AMS was operated only in V mode with 10 sec  
186 time resolution. Several ionization efficiency calibrations performed prior to and during the field  
187 campaign varied by <10 %. To determine the AMS collection efficiency, number concentrations  
188 measured by an Ultra High Sensitivity Aerosol Spectrometer (UHSAS; Droplet Measurement  
189 Technologies Inc.) over a size range of 60 nm to 1 µm were converted to volume concentrations using  
190 mid-point bin diameters and assuming spherical shapes. ~~Volume concentrations were converted to mass~~  
191 ~~concentrations using densities weighted by the AMS chemical components~~ Total mass was calculated  
192 from the UHSAS measurements based on the composition-weighted proportional density determined  
193 from the AMS. A collection efficiency of 0.5 was determined. Detailed investigations and discussions  
194 around the collection efficiency of the AMS can be found in the literature (Middlebrook et al., 2012;  
195 Dunlea et al., 2009; Kleinman et al., 2008; Drewnick et al., 2004; Quinn et al., 2006). PM<sub>1</sub> is the sum of  
196 the mass concentrations of AMS components (OA, NO<sub>3</sub>, SO<sub>4</sub> and NH<sub>4</sub>). ~~The PM<sub>1</sub> from this study is~~  
197 ~~compared with the For comparisons of PM<sub>1</sub> from this study and PM<sub>2.5</sub> EFs from the Andreae (2019)~~  
198 ~~literature review of boreal forest wildfire studies. While these measurements represent PM over different~~  
199 ~~size ranges (< 1µm vs <2.5µm), the difference is not expected to be significant based on typical size~~  
200 ~~distributions of wildfire emissions (Andreae 2019; Reid and Hobbs, 1998; Reid et al., 2005). This~~  
201 ~~approach has been used previously in literature reviews of EFs for wildfire emissions (Andreae 2019;~~  
202 ~~Akagi et al., 2011). other studies, the mass was estimated between 1 and 2.5 µm to assess the extent of~~  
203 ~~which this might be influencing such comparisons. Using estimated particle mass concentrations from a~~  
204 ~~Fast Cloud Droplet Probe (FCDP) (<2.5 µm) and those from a UHSAS (<1 µm), there is an estimated~~  
205 ~~10 % of aerosol mass between 1 and 2.5 µm.~~

206 **BC** The SP2 (~~Droplet Measurement Technologies~~) measures the mass of rBC contained in individual  
207 aerosols through the laser-induced incandescence of heated rBC-containing aerosols (Stephens et al.,  
208 2003; Baumgardner et al., 2004; Schwarz et al., 2006). The SP2 was calibrated using fullerene soot  
209 (Alpha Aesar lot# F12S011) (Moteki and Kondo, 2010; Kondo et al., 2011; Laborde et al., 2012)  
210 nebulized from a water suspension and passed through an aerosol particle mass analyzer (Kanomax  
211 APM3600) to select particles with masses ranging from 0.2 fg/particle to 48 fg/particle. Extremely large  
212 particles containing more than 520 fg of rBC were excluded from analysis due to saturation of the  
213 detector (these accounted for only  $2 \times 10^{-3}$  % of the total number of rBC containing particles measured by  
214 the SP2).

215 **UHSAS** Particle size distributions were measured using an Ultra-High Sensitivity Aerosol Spectrometer  
216 (~~UHSAS; Droplet Measurement Technologies~~). The UHSAS measures the size of individual aerosols  
217 passing through a laser beam via Mie scattering (Cai et al., 2008; Kupc et al., 2018). These particles are  
218 classified into 99 log-normally spaced bins across the measurement range. Periods where the particle  
219 concentration measured by the UHSAS exceeded 3000 particles  $s^{-1}$  were excluded from this analysis due  
220 to the potential of coincident particles passing through the laser beam. The UHSAS particle sizing was  
221 verified using NIST traceable polystyrene latex (PSL) nanospheres of multiple sizes across the  
222 measurement range. Total particle mass was calculated from the UHSAS measurements assuming a  
223 density of  $1.2 \text{ g cm}^{-3}$ , based on the **composition-weighted** proportional density determined from the AMS.

### 224 **12.1.3 Identification of organic compounds**

225 Three methods were used to provide detailed measurements of gas-phase organic compounds that  
226 included the PTRMS, CIMS, and canister samples (AWAS). The PTRMS and CIMS are able to resolve  
227 the molecular formula of isobaric species, but cannot distinguish isomers, while the AWAS system can  
228 identify and speciate individual compounds. For the PTRMS measurements, compound molecular  
229 formulae were assigned based on a limited set of possibilities (particularly for the smaller compounds),  
230 known or expected compound sensitivities, and comparing with previously published laboratory work by

231 Koss et al. (2018) based on typical NMOG structures observed in biomass burning emissions. Koss et al.  
232 (2018) used a combination of gas-chromatography (GC) pre-separation,  $\text{NO}^+$  CIMS and time series  
233 correlations to identify 156 compounds measured in biomass burning laboratory experiments with a  
234 PTRMS. Additional comparisons were made with PTRMS ion masses reported in Permar et al. (2021)  
235 where they used a PTRMS with two GC methods to speciate isomers for some PTRMS ion masses. For  
236 formulas with multiple isomer contributions that were not speciated by the PTRMS, or provided by the  
237 AWAS, the fractional contributions in Koss et al. (2018) and Permar et al. (2021) were used to identify  
238 the dominant ion and/or contributing compounds. Although the Koss et al. (2018) work was based on  
239 laboratory measurements, Permar et al. (2021) found that isomer contributions did not vary much between  
240 24 fires types across the WE-CAN airborne field campaign in western US, which were mainly dominated  
241 by fires of pine, fir and spruce trees. For example, in Koss et al. (2018), for the mass spectral ion of  
242  $\text{C}_3\text{H}_6\text{O}$  ( $m/z$  58.08), the contribution from acetone was set at 100 % and propanal 0 %, only slightly  
243 different from the contribution of  $83 \pm 6$  % for acetone determined by Permar et al., 2021; thus this  
244 compound was identified as acetone in this work. Another example is  $\text{C}_4\text{H}_8\text{O}$  at  $m/z$  70.091 that has  
245 potential contributions from methyl vinyl ketone (MVK), methacrolein and crotonaldehyde, both Koss et  
246 al. (2018) and Permar et al. (2021) both reported that MVK is the largest contributor at 48 % and  $60 \pm 9$  %  
247 respectively; the compound was labelled here as all three. For  $\text{C}_8\text{H}_{10}$  ( $m/z$  106.168), there are  
248 contributions from ethyl-benzene, m- and p-xylenes and o-xylene identified as 10%, 68% and 23%,  
249 respectively (Koss et al., 2018), with slightly different isomer contributions as per Permar et al. (2021).  
250 In this study, as it was not possible to speciate  $\text{C}_8\text{H}_{10}$  with the AWAS system, it is simply identified as C8  
251 aromatics. Similarly,  $\text{C}_{10}\text{H}_{16}$ , ( $m/z$  136.238) is identified as total monoterpenes in the present study, with  
252 expected contributions from multiple species including alpha and beta pinene, camphene, myrcene, and  
253 tricyclene (Permar et al., 2021; Hatch et al., 2017).  $\text{C}_5\text{H}_8$  at  $m/z$  68.119 was identified as isoprene in the  
254 present study, recognizing that there may be a fractional contribution to this mass from methyl-3-buten-2-  
255 ol (MBO), although Permar et al. (2021), suggests that MBO may not be significant, based on their  
256 analysis of western US wildfires.

257 For the CIMS, the iodide reagent ion chemistry is most sensitive to polar compounds, particularly  
258 carboxylic acids and less sensitive to non-polar compounds (Table S1). Compounds were identified using  
259 these known/expected sensitivities and available calibration standards. The AWAS provided speciated  
260 measurements of hydrocarbons ( $\leq C_{10}$ ), and no oxygenates.

261  
262 **12.1.4 Overlapping compounds** There were a number of compounds (or molecular formulae) that were  
263 measured by both the PTRMS and the AWAS, as well as compounds that overlapped between the  
264 PTRMS and CIMS. Tables S4 and S5 summarize the decisions of overlapping compounds that were  
265 retained for derivation of EFs and NERs, as well as for the carbon/nitrogen budget analyses. For the  
266 PTRMS and AWAS, for some molecular formulae, the AWAS provided measurements of individual  
267 isomers, while the corresponding PTRMS measurement was expected to reflect ~~the sum of these some~~  
268 ~~quantity of the sum of multiple~~ isomers. Comparisons between these two methods are challenging due to  
269 the influence of isomers in the PTRMS signal, and the fact that a number of the PTRMS compounds are  
270 determined using calculated sensitivities (i.e. not directly calibrated with a standard) with estimated  
271 uncertainties of 50 %. These factors limit a comparison between the AWAS and PTRMS for isoprene  
272 ( $C_5H_8$ ) which is shown in Fig. S3a. The comparison for Screens 1 through 3 shows good agreement with  
273 an  $r^2=0.87$ . When including only Screen 1 data, there are two data points (in the SP) where the PTRMS is  
274 a factor of 2.5 to 3 higher than the AWAS, resulting in a lower  $r^2=0.45$ . Although the PTRMS isoprene  
275 signal is known to have interferences from cycloalkanes, these compounds are not expected to be emitted  
276 from wildfires. 2-methyl-3-buten-2-ol (MBO) produces a fragment at  $m/z$  69.070 that is not separated in  
277 the PTRMS, and can also interfere with the isoprene measurement. We do not have measurements to  
278 confirm the impact of MBO on the isoprene signal. However, Permar et al. (2021) reported that PTRMS  
279 derived isoprene measurements during their study were approximately 2x higher than the AWAS isoprene  
280 while sampling smoke, but MBO which was measured during that study was considered too low to  
281 account for the higher than expected isoprene. In the present study, it is possible that there were  
282 contributions from other unknown isomers to the PTRMS signal in the fresh smoke plumes along Screen

283 1. Due to these uncertainties, and the comparatively fewer in-plume AWAS samples, EFs and ERs for  
284 isoprene are reported from both the PTRMS and AWAS, and isoprene from the PTRMS was used in the  
285 carbon budget (Table S4).

286 In deriving EFs and ~~NERs~~, both the PTRMS and AWAS measurements were included to retain as  
287 much information as possible. To avoid double-counting compounds in the carbon and nitrogen budget  
288 analyses, only the PTRMS measurement was typically included as it is expected to reflect a sum of ~~all~~  
289 ~~multiple~~ isomers, thus, accounting for more carbon. For example, at the molecular formulas of C<sub>5</sub>H<sub>10</sub>, the  
290 PTRMS measurements are expected to reflect the sum of all the isomers, whereas ~~5-7~~ compounds were  
291 speciated from the AWAS i.e. c-2-pentene, cyclopentane, 1-pentene, 2-me-1-butene, ~~3-methyl-1-butene,~~  
292 ~~t-2 pentene,~~ and 2-me-2-butene. In this case, EFs and ~~NERs~~ were derived for both the PTRMS and  
293 AWAS measurements, but only the PTRMS measurements were included in the budget analyses.

294 Between the PTRMS and CIMS, there were 18 overlapping molecular formulae. ~~Although~~  
295 ~~comparisons of exact masses between the PTRMS and CIMS are complicated because of the influence of~~  
296 ~~isomers in the PTRMS signal, four exact masses of which 4 were identified as the same compound~~  
297 ~~including acetic acid, acrylic acid, formic acid, and isocyanic acid. Figure S3 shows a comparison for the~~  
298 ~~first three compounds, but excludes isocyanic acid as this compound can hydrolyze in the PTRMS drift~~  
299 ~~tube. The CIMS provided measurements of pyruvic acid, but the PTRMS signal at the same mass is~~  
300 ~~likely affected by inlet line losses. Acetic acid and acrylic acid show good agreement with  $r^2 > 0.8$  with~~  
301 ~~the PTRMS in-plume measurements ~20 % higher than the CIMS (Fig. S3a, b); this is likely due to~~  
302 ~~additional contributions to the PTRMS signal at these respective exact masses. The comparison for~~  
303 ~~formic acid (Fig. S3c) is poor ( $r^2 = 0.3$ ) likely because the PTRMS measurements are noisy and have a~~  
304 ~~high detection limit of 2 ppbv, whereas the CIMS detection limit is 0.097 ppbv. The CIMS~~  
305 ~~measurements were also directly calibrated (Table S2), whereas the PTRMS formic acid sensitivity (and~~  
306 ~~other compounds) were calculated, and as such, the CIMS measurements for the overlapping compounds~~  
307 ~~were retained for analysis f(Table S5). ~~or 3 of these 4 compounds (Table S5) because they were directly~~~~  
308 ~~calibrated (Table S2), whereas the PTRMS compounds were calculated. For the 4<sup>th</sup> compound (acetic~~

309 acid), EFs for both instruments were reported, but only the CIMS data for acetic acid were included in the  
310 carbon budget analyses; EFs were very similar (Table A1). The remaining overlapping formulae between  
311 the CIMS and PTRMS were calibrated with different analytes, and thus assumed to be different species.  
312 While there may in fact be some overlap between isomers contributing to these formulae, their overall  
313 contribution to the TC budget is small (<4 %). An attempt was made to quantify as many other peaks that  
314 were present in the CIMS mass spectra as possible and apply sensitivity factors. However, the available  
315 sensitivity factors were based on laboratory experiments investigating anthropogenic emissions and  
316 highly uncertain for biomass burning measurements. Nevertheless, application of these sensitivity factors  
317 resulted in average mass from the CIMS spectra totalling < 1.5 % of the TC, so although uncertain,  
318 exclusion of these masses is not expected to significantly influence the total carbon budget. It is assumed  
319 that all the acids measured by the CIMS are non-aromatic for classifying into chemical structural  
320 categories.

321

## 322 **1.2 Mass balance method for estimating aircraft-derived emission rates**

323 The Topdown Emission Rate Retrieval Algorithm (TERRA) was designed to estimate emission rates of  
324 pollutants measured by aircraft. The algorithm is based on the Divergence Theorem to achieve mass  
325 balance and been extensively applied to a range of pollutants measured by aircraft (e.g. Hayden et al.,  
326 2021; Baray et al., 2018; Li et al., 2017; Liggió et al., 2017; Gordon et al., 2015). An extension of  
327 TERRA previously used for estimating pollutant mass transfer rates across virtual aircraft screens (e.g.  
328 Hayden et al., 2021; Baray et al., 2018) was used in the present study to estimate emission rates of NO<sub>x</sub>,  
329 CO, PM<sub>1</sub> and NH<sub>3</sub> using Screen 1 data. Briefly, pollutant concentrations and horizontal wind speeds were  
330 mapped to virtual screens and interpolated using a kriging function, as well as extrapolating the  
331 measurements from the lowest aircraft altitude to the surface using applicable extrapolation profiles.  
332 Mass transfer rates were derived by integration of the horizontal fluxes across the plume on the screen in

333 units of  $\text{t h}^{-1}$ . The main uncertainty in the mass transfer rate is due to extrapolation to the surface as  
334 described previously (e.g. Gordon et al., 2015 and Hayden et al., 2021).

335

### 336 **2.22.0 Flight and fire description**

337 The 18BN-Larry fire (the Lac LaLoche fires) was detected by the Saskatchewan wildfire  
338 management agency on June 23, 2018. Satellite images showed fire hot spots on June 23 and by the  
339 evening of June 23 it grew to 1,250 hectares (ha) and to 2,600 ha on June 24<sup>th</sup>. On the morning of June  
340 25, 2018, there was a very weak nocturnal inversion and moderately strong south to southeast winds at 33  
341 knots above the inversion. The range of fire intensities during the previous night, as well as the observed  
342 high humidity (80-90 %) and light to moderate winds observed at the surface also indicates that the fire  
343 source at the time of aircraft sampling was in a smoldering combustion state. Flight tracks were flown at  
344 Lagrangian distances downwind of the wildfire. Multiple passes (i.e. transects) perpendicular to the  
345 plume direction were made at different altitudes. Two plumes were identified: the SP was clearly due to  
346 the fire hot spots identified by MODIS (green dots encompassed by a polygon), but the source of the NP  
347 is less certain. It is possible that MODIS was unable to detect the fire source because the fire heat  
348 signature was below the threshold for satellite instrument detection. However, surface wind  
349 measurements at Lac LaLoche (SI Table S1 in McLagan et al., 2021) show that the wind direction was  
350 southerly just prior (approx. 30 min) to the start of the aircraft measurements, and then shifted to  
351 southeast ( $135 \pm 13^\circ$ ) for the duration of the aircraft flight. Therefore, it is likely that the NP was from  
352 the same fire source as the SP that had been transported in a northerly direction just prior to aircraft  
353 sampling, and subsequently moved to a northwesterly direction with the wind change. The width of the  
354 SP and NP was approximately 14-37 km separated by approximately 8-19 km depending on the sampling  
355 altitude, and with an aircraft speed of  $\sim 90 \text{ m s}^{-1}$ , the plumes were traversed in 3-7 min (Fig. 2).

356

### 357 **~~3 Emission ratios, emission factors and combustion efficiency~~**

### 358 **3.01 Combustion state**

359           The combustion efficiency (CE) can be used to characterize and compare the combustion state of  
360 the fire, (i.e. the fraction of fuel carbon converted to atmospheric CO<sub>2</sub>) (Ward and Radke, 1993). The CE  
361 is dependent upon many factors including fire combustion state, fuel chemistry, fuel geometry, growth  
362 stage, moisture content and meteorological conditions such as wind speed and temperature. In a flaming  
363 fire, high temperature reactions tend to go to completion (>90 %) as rapid reaction of O<sub>2</sub> with the fuel C,  
364 H, N and S produces highly oxidized gases including CO<sub>2</sub>, NO<sub>x</sub>, and SO<sub>2</sub> and BC. As a fire progresses,  
365 incomplete combustion characteristics of smoldering fires becomes more dominant resulting in a larger  
366 proportion of the emitted carbon in the form of CO, CH<sub>4</sub>, NMOC, and OA. Airborne measurements tend  
367 to sample a mixture of combustion states; however, there tends to be a dominant phase of combustion at  
368 different fire stages (Andreae and Merlet, 2001). If only accounting for CO<sub>2</sub> and CO, the MCE for the SP  
369 is 0.90±0.01 and NP is 0.88±0.01, higher than the CE by 7.1 % and 6.6 % for the SP and NP,  
370 respectively. These differences are driven mostly by the additional contribution from NMOGs indicating  
371 the importance of their inclusion in assessing fire combustion state.

372           Since the flaming phase was likely more than 14 hrs prior to aircraft sampling, it is possible that  
373 the emissions from this fire may also reflect a residual smoldering combustion (RSC) component. RSC  
374 produces emissions from combustion of forest floor and woody debris that are not associated with  
375 flaming, can be sustained for long periods of time after the passage of a flame front, and are not strongly  
376 lofted through fire-induced convection (Bertschi et al., 2003). It is noted though that observations of  
377 increased levels of flaming compounds in the plumes including CO<sub>2</sub> and BC (Fig. S42) suggest that to  
378 some extent, flaming processes also contributed to the release of these compounds. It is likely that  
379 different parts of the fire had varying mixtures of smoldering, flaming and residual combustion processes,  
380 but the evidence strongly suggests that the Lac LaLoche fire was predominantly in a smoldering  
381 combustion state during the aircraft measurement time period. Smoldering fires can create persistent and  
382 poorly ventilated smoke that can be a significant driver in remote community evacuations (McGee, 2020).

383 In addition, boreal fires in this region tend to exhibit a large component of smoldering combustion which  
384 can consume large amounts of above and below ground biomass (Akagi et al., 2011).

385

386 Table S1. Measurements with associated instrument, principle of operation, sampling time resolution,  
 387 uncertainty, detection limit, and applicable method references.

Measurement	Instrument	Principle of measurement	Time Resolution (sec)	Uncertainty	Detection Limit	Reference
NO	Thermo 42i	Chemiluminescence with O <sub>3</sub>	1	±5 %	3σ at 1 sec 0.17 ppbv	Clyne et al., 1964 Ridley et al., 1990
NO <sub>2</sub>	Thermo 42i	Photolysis + chemiluminescence with O <sub>3</sub>	1	±7 %	3σ at 1 sec 0.43 ppbv	Penkett et al., 2011
NO <sub>y</sub>	Thermo 42i	Heated (350°C) and molybdenum catalyzed conversion + chemiluminescence with O <sub>3</sub>	1	±5 %	3σ at 1 sec 0.18 ppbv	Fehsenfeld et al., 1987; Williams et al., 1998
SO <sub>2</sub>	Thermo 43i	UV pulsed fluorescence	1	±5 %	3σ at 1 sec 1.25 ppbv	Stecher et al., 1997
O <sub>3</sub>	Thermo 42i	Chemiluminescence	1	±5 %	3σ at 1 sec 0.52 ppbv	N/A
NH <sub>3</sub>	LGR model 911-0039	Absorption	1	±5 %	2.1 ppbv at 1 sec 0.3 ppbv at 60 sec	Leifer et al., 2017
Hg (GEM)	Tekran 237X	Fluorescence	120	±0.054 ng m <sup>-3</sup>	<0.1 ng m <sup>-3</sup>	Cole et al., 2014; McLagan et al., 2021
CO, CO <sub>2</sub> , CH <sub>4</sub>	Picarro G-2401-m	Cavity ring down spectrometry	2	CH <sub>4</sub> ~±3 ppbv	N/A	Baray et al., 2018
Total Carbon (TC)	Picarro G-2401-m	Heated (650°C) platinum catalyzed conversion to CO <sub>2</sub>	2	3σ at 10 sec ±60 ppbv	N/A	Stockwell et al., 2018; Veres et al., 2010.
Total non-methane organic gases (NMOG <sub>T</sub> )	Picarro G-2401-m x 2	Difference method, heated (650°C) platinum catalyzed conversion to CO <sub>2</sub>	10	3σ at 10 sec ±85 ppbv	85 ppbv 3σ at 10 sec	Stockwell et al., 2018; Veres et al., 2010
VOCs	CIMS	Chemical ionization/mass spectrometry	1	±10-50% compound dependent	See Table S2	Liggio et al., 2017; Lee et al., 2014
VOCs (≤C10)	<del>Canister grab samples (AWAS)</del>	Grab samples/GC with MS and FID analysis	<del>Grab20-30</del>	<C <sub>6</sub> ±25% ≥C <sub>6</sub> ±40-%	0.7 to 12.9 pptv for compounds from C <sub>2</sub> to C <sub>8</sub> ; 1 to 242 pptv for C <sub>9</sub> and C <sub>10</sub> compounds	N/A
VOCs	PTRMS	Proton transfer/ionization/mass spectrometry	1	VOCs with available standards: ±15% except CH <sub>2</sub> O at- ±20%; Calculated	Range of 0.005 to 1 ppbv, CH <sub>2</sub> O 4.6 ppbv at 1 sec	Li et al., 2017; Sekimoto et al., 2017

				VOCs: ±50%		
VOCs-SVOCs (C10-C25)	Custom packed adsorbent tubes	Offline analysis with TD- GC-APCI-Q-ToF	Variable (245-3140 sec per tube)		1 ppt	Sheu et al., 2018; Khare et al., 2019; Ditto et al., 2021
Particle chemical composition	Aerosol mass spectrometer	Volatilization, ionization and mass spectrometry	10	OA: ±35% SO <sub>4</sub> : ±25% NO <sub>3</sub> : ±20% NH <sub>4</sub> : ±25%	OA: 0.24 µg m <sup>-3</sup> SO <sub>4</sub> : 0.05 µg m <sup>-3</sup> NO <sub>3</sub> : 0.035 µg m <sup>-3</sup> NH <sub>4</sub> : 0.15 µg m <sup>-3</sup> at 10 sec	DeCarlo et al., 2008; Jimenez et al., 2003; Allan et al., 2003
Black carbon	SP2	Incandescence	1	15 %	0.01 µg m <sup>-3</sup> at 1 sec	Stephens et al., 2003; Baumgardner et al., 2004; Schwarz et al., 2006
Particle size distributions (60 -1000 nm)	Ultra-High Sensitivity Aerosol Spectrometer (UHSAS)	Particle light scattering	1	10 %		Cai et al., 2008; Kupc et al., 2018

388

389

390

391

392

393

394

395

396

397

398

399

400

401

402

403

404

405 Table S2. Standards used to calibrate the CIMS, as well as the compound uncertainty, detection limit and  
 406 applicable method reference. The iodide chemistry is most sensitive to polar compounds and less  
 407 sensitive to non-polar compounds. The sensitivity tends to increase for keto-, hydroxy- and acid groups,  
 408 in order. Most of the keto- groups are attached to a carboxylic acid. For the larger acids (>C4) where there  
 409 can be several isomers, they are generally identified as saturated C4 carboxylic acids and unsaturated C5  
 410 acids.

Molecular weight	Molecular formula	Compound Name	Calibration standard	Calibration Source	Uncertainty (%)	Detection Limit (pptv)	Reference
27.026	HCN	hydrogen cyanide	Hydrogen Cyanide	High Pressure Cylinder (Air Liquide)	20	17	Stockwell et al 2018
32.06	SO <sub>2</sub>	sulphur dioxide	Sulfur Dioxide	High Pressure Cylinder (Air Liquide)	N/A	N/A	Lee et al 2018
43.025	HNCO	isocyanic acid	Isocyanic Acid	Thermal Decomposition/ Diffusion	30	10	Roberts et al 2010
46.025	CH <sub>2</sub> O <sub>2</sub>	formic acid	Formic Acid	Liquid Standard supplied by Liquid Calibration Unit (LCU)	20	156	Mungall et al 2017
47.013	HONO	nitrous acid	Nitrous Acid	Acid Displacement (output quantified by ion chromatography )	30	12	Roberts et al 2010
57.052	C <sub>2</sub> H <sub>3</sub> NO	hydroxy acetonitrile	Glycolic Acid Nitrile	Liquid Standard supplied by Liquid Calibration Unit (LCU)	20	0.12	Mungall et al 2017
60.052	C <sub>2</sub> H <sub>4</sub> O <sub>2</sub>	acetic acid	Acetic Acid	Liquid Standard supplied by Liquid Calibration Unit (LCU)	20	576	Mungall et al 2017
63.012	HNO <sub>3</sub>	nitric acid	Nitric Acid	Permeation Tube (output quantified by ion chromatography )	N/A	58	Neuman et al 1999
72.063	C <sub>3</sub> H <sub>4</sub> O <sub>2</sub>	acrylic acid	Acrylic Acid	Liquid Standard supplied by Liquid Calibration Unit (LCU)	20	17	Mungall et al 2017
74.079	C <sub>3</sub> H <sub>6</sub> O <sub>2</sub>	propionic acid	Propionic Acid	Liquid Standard supplied by Liquid	20	55	Mungall et al 2017

				Calibration Unit (LCU)			
79.011	HNO <sub>4</sub>	pernitric acid	Pernitric Acid	Reaction of HO <sub>2</sub> with NO <sub>2</sub> (quantified by thermal decomposition Cavity Ringdown Spectroscopy of NO <sub>2</sub> )	50	2	Veres et al 2015
84.074	C <sub>4</sub> H <sub>4</sub> O <sub>2</sub>	C <sub>4</sub> H <sub>4</sub> O <sub>2</sub>	2(5H)-Furanone	Liquid Standard supplied by Liquid Calibration Unit (LCU)	20	51	Mungall et al 2017
85.062	C <sub>3</sub> H <sub>3</sub> NO <sub>2</sub>	Cyanoacetic acid	Cyanoacetic Acid	Liquid Standard supplied by Liquid Calibration Unit (LCU)	20	0.17	Mungall et al 2017
86.09	C <sub>4</sub> H <sub>6</sub> O <sub>2</sub>	methacrylic acid	Methacrylic Acid	Liquid Standard supplied by Liquid Calibration Unit (LCU)	N/A	N/A	Mungall et al 2017
88.062	C <sub>3</sub> H <sub>4</sub> O <sub>3</sub>	pyruvic acid	Pyruvic Acid	Liquid Standard supplied by Liquid Calibration Unit (LCU)	20	253	Mungall et al 2017
88.106	C <sub>4</sub> H <sub>8</sub> O <sub>2</sub>	C4 saturated carboxylic acids	Butyric Acid	Liquid Standard supplied by Liquid Calibration Unit (LCU)	20	63	Mungall et al 2017
91.066	C <sub>2</sub> H <sub>5</sub> NO <sub>3</sub>	C2 Nitro alcohol	2-Nitroethanol	Liquid Standard supplied by Liquid Calibration Unit (LCU)	20	0.80	Mungall et al 2017
100.117	C <sub>5</sub> H <sub>8</sub> O <sub>2</sub>	unsaturated C5 carboxylic acids	4-Pentenoic Acid	Liquid Standard supplied by Liquid Calibration Unit (LCU)	20	19	Mungall et al 2017
102.089	C <sub>4</sub> H <sub>6</sub> O <sub>3</sub>	C4 oxo-carboxylic acids	2-Ketobutyric Acid	Liquid Standard supplied by Liquid Calibration Unit (LCU)	20	354	Mungall et al 2017
102.133	C <sub>5</sub> H <sub>10</sub> O <sub>2</sub>	C5 saturated carboxylic acids	Valeric Acid + Isovaleric Acid (equal parts)	Liquid Standard supplied by Liquid	20	46	Mungall et al 2017

				Calibration Unit (LCU)			
104.105	C <sub>4</sub> H <sub>8</sub> O <sub>3</sub>	C4 hydroxy-carboxylic acids	3-Hydroxybutyric Acid	Liquid Standard supplied by Liquid Calibration Unit (LCU)	20	4	Mungall et al 2017
108.009	N <sub>2</sub> O <sub>5</sub>	dinitrogen pentoxide	Dinitrogen Pentaoxide	Titration of NO <sub>2</sub> with O <sub>3</sub> (quantified by thermal decomposition Cavity Ringdown Spectroscopy of NO <sub>2</sub> )	50	0.14	Lee et al 2018
114.144	C <sub>6</sub> H <sub>10</sub> O <sub>2</sub>	sum of cyclic saturated and n-unsaturated C5 carboxylic acids	Cyclopentanecarboxylic Acid	Liquid Standard supplied by Liquid Calibration Unit (LCU)	20	28	Mungall et al 2017
116.116	C <sub>5</sub> H <sub>8</sub> O <sub>3</sub>	C5 oxo-carboxylic acids	Levulinic Acid	Liquid Standard supplied by Liquid Calibration Unit (LCU)	20	11	Mungall et al 2017
116.16	C <sub>6</sub> H <sub>12</sub> O <sub>2</sub>	C6 saturated carboxylic acids	Hexanoic Acid + 4-Methyl-Valeric Acid (equal parts)	Liquid Standard supplied by Liquid Calibration Unit (LCU)	20	13	Mungall et al 2017
118.132	C <sub>5</sub> H <sub>10</sub> O <sub>3</sub>	C5 hydroxy-carboxylic acids	2-Hydroxy-2-methylbutyric Acid	Liquid Standard supplied by Liquid Calibration Unit (LCU)	20	59	
126.155	C <sub>7</sub> H <sub>10</sub> O <sub>2</sub>	unsaturated C6 cyclic carboxylic acid	3-Cyclohexene-1-carboxylic Acid	Liquid Standard supplied by Liquid Calibration Unit (LCU)	20	6	
128.171	C <sub>7</sub> H <sub>12</sub> O <sub>2</sub>	C6 unsaturated carboxylic acids	6-Heptenoic Acid	Liquid Standard supplied by Liquid Calibration Unit (LCU)	20	11	
130.187	C <sub>7</sub> H <sub>14</sub> O <sub>2</sub>	C7 saturated carboxylic acids	Heptanoic Acid	Liquid Standard supplied by Liquid Calibration Unit (LCU)	20	23	
132.159	C <sub>6</sub> H <sub>12</sub> O <sub>3</sub>	C6 hydroxy-carboxylic acids	2-Hydroxyisocaproic Acid	Liquid Standard supplied by Liquid	20	1.6	

				Calibration Unit (LCU)			
--	--	--	--	---------------------------	--	--	--

411

412

413 Table S3. Standards used to calibrate the PTRMS. <sup>a</sup>C8 aromatics - expected contributions from ethyl  
 414 benzene, m- and p-xylenes and o-xylene. <sup>b</sup>Monoterpenes - expected contributions from camphene,  $\alpha$ -  
 415 pinene,  $\beta$ -pinene, myrcene, and tricyclene.  
 416

<b>Molecular weight</b>	<b>Molecular formula</b>	<b>Compound Name</b>	<b>Calibration standard</b>
30.026	CH <sub>2</sub> O	formaldehyde	formaldehyde
32.042	CH <sub>4</sub> O	methanol	methanol
34.076	H <sub>2</sub> S	hydrogen sulfide	hydrogen sulfide
41.053	C <sub>2</sub> H <sub>3</sub> N	acetonitrile	acetonitrile
44.053	C <sub>2</sub> H <sub>4</sub> O	acetaldehyde	acetaldehyde
56.064	C <sub>3</sub> H <sub>4</sub> O	acrolein	acrolein
58.08	C <sub>3</sub> H <sub>6</sub> O	acetone	acetone
62.13	C <sub>2</sub> H <sub>6</sub> S	dimethyl sulfide	dimethyl sulfide
68.119	C <sub>5</sub> H <sub>8</sub>	isoprene	isoprene
70.091	C <sub>4</sub> H <sub>6</sub> O	MVK, methacrolein, crotonaldehyde	crotonaldehyde
72.107	C <sub>4</sub> H <sub>8</sub> O	MEK, 2-methyl acetate, ethyl formate	methylethyl ketone
76.157	C <sub>3</sub> H <sub>8</sub> S	2-propanethiol, ethyl methyl sulfide	ethylmethyl sulfide
78.114	C <sub>6</sub> H <sub>6</sub>	benzene	benzene
84.136	C <sub>4</sub> H <sub>4</sub> S	thiophene	thiophene
90.184	C <sub>4</sub> H <sub>10</sub> S	diethyl sulfide, butanethiol	diethyl sulfide
92.141	C <sub>7</sub> H <sub>8</sub>	toluene	toluene
98.163	C <sub>5</sub> H <sub>6</sub> S	methyl thiophene	2-methylthiophene
106.168	C <sub>8</sub> H <sub>10</sub>	C8 aromatics <sup>a</sup>	o-xylene
112.19	C <sub>6</sub> H <sub>8</sub> S	dimethylthiophene	2,3-dimethylthiophene
136.238	C <sub>10</sub> H <sub>16</sub>	monoterpenes <sup>b</sup>	camphene

417

418 Table S4. Overlapping compounds measured between the PTRMS and AWAS.

Molecular Weight	Formula	Compound Name	Instrument	Decision for budget	Decision for EFs
42.081	C <sub>3</sub> H <sub>6</sub>	propene	AWAS and PTRMS	AWAS	AWAS
54.092	C <sub>4</sub> H <sub>6</sub>	butadiene/fragments	PTRMS	PTRMS	PTRMS and AWAS
		1,3-butadiene	AWAS		
56.108	C <sub>4</sub> H <sub>8</sub>	butenes	PTRMS	AWAS	AWAS
		cis-2-butene	AWAS		
		isobutene	AWAS		
		trans-2-butene	AWAS		
		1-butene	AWAS		
58.124	C <sub>4</sub> H <sub>10</sub>	butanes	PTRMS	AWAS	AWAS
		<del>isobutane</del>	<del>AWAS</del>		
		n-butane	AWAS		
<del>68.119</del>	<del>C<sub>5</sub>H<sub>8</sub></del>	<del>isoprene</del>	<del>PTRMS and AWAS</del>	<del>PTRMS</del>	<del>PTRMS and AWAS</del>
70.135	C <sub>5</sub> H <sub>10</sub>	pentene/fragments	PTRMS	PTRMS	PTRMS and AWAS
		cis-2-pentene	AWAS		
		cyclopentane	AWAS		
		1-pentene	AWAS		
		2-methyl-1-butene	AWAS		
		2-methyl-2-butene	AWAS		
		<del>3-methyl-1-butene</del>	<del>AWAS</del>		
		<del>t-2 pentene</del>	<del>AWAS</del>		
<del>78.114</del>	<del>C<sub>6</sub>H<sub>6</sub></del>	<del>benzene</del>	<del>PTRMS and AWAS</del>	<del>PTRMS</del>	<del>PTRMS</del>
82.146	C <sub>6</sub> H <sub>10</sub>	cyclohexene	PTRMS and AWAS	PTRMS	PTRMS
84.162	C <sub>6</sub> H <sub>12</sub>	hexene	<del>PTRMS and AWAS</del>	PTRMS ( <del>hexane</del> ) AWAS ( <del>cyclohexane</del> )	PTRMS and ( <del>hexane</del> ) AWAS ( <del>cyclohexane</del> ) AWAS
		cyclohexane	AWAS		
		<del>cis-2-hexene</del>	<del>AWAS</del>		
86.178	C <sub>6</sub> H <sub>14</sub>	hexanes	<del>PTRMS and AWAS</del>	AWAS	AWAS
		n-hexane	AWAS		
		2,3-dimethyl butane	AWAS		
		2,3-dimethylpentane	AWAS		

419

420

421 Table S5. Overlapping compounds measured between the PTRMS and CIMS. <sup>a</sup>The PTRMS signal at  
 422 molecular weight 60.052 is reported as acetic acid fragment; the signal can also be due to glycoaldehyde  
 423 (Koss et al., 2018), but the PTRMS and CIMS acetic acid mixing ratios and EFs match each other closely  
 424 suggesting that the PTRMS fragment is mostly due to acetic acid.

Molecular weight	Formula	CIMS compound name	PTRMS compound name	Decision
43.025	HNCO	Isocyanic acid	Isocyanic acid	CIMS and PTRMS for reporting EF and ER; CIMS for carbon budget
46.025	CH <sub>2</sub> O <sub>2</sub>	Formic acid	Formic acid	CIMS
57.052	C <sub>2</sub> H <sub>3</sub> NO	Hydroxy acetonitrile	Methyl isocyanate	CIMS and PTRMS
60.052	C <sub>2</sub> H <sub>4</sub> O <sub>2</sub>	Acetic acid	Acetic acid fragment <sup>a</sup>	CIMS and PTRMS for reporting EF and ER; CIMS for carbon budget
72.063	C <sub>3</sub> H <sub>4</sub> O <sub>2</sub>	Acrylic acid	Methyl glyoxal/acrylic acid	CIMS
74.079	C <sub>3</sub> H <sub>6</sub> O <sub>2</sub>	Propionic acid	Hydroxy acetone/ethyl formate	CIMS and PTRMS
84.074	C <sub>4</sub> H <sub>4</sub> O <sub>2</sub>	Unidentified	Furanone	CIMS and PTRMS
85.062	C <sub>3</sub> H <sub>3</sub> NO <sub>2</sub>	Cyanoacetic acid	Methyl cyanofomate	CIMS and PTRMS
86.09	C <sub>4</sub> H <sub>6</sub> O <sub>2</sub>	Methacrylic acid	Butanedione/isomers	CIMS and PTRMS
<del>88.062</del>	<del>C<sub>3</sub>H<sub>4</sub>O<sub>3</sub></del>	<del>Pyruvic acid</del>	<del>Pyruvic acid</del>	<del>CIMS</del>
88.106	C <sub>4</sub> H <sub>8</sub> O <sub>2</sub>	C4 saturated carboxylic acids	Methyl propanoate	CIMS and PTRMS
100.117	C <sub>5</sub> H <sub>8</sub> O <sub>2</sub>	Unsaturated C5 carboxylic acids	Methyl methacrylate/isomers	CIMS and PTRMS
102.089	C <sub>4</sub> H <sub>6</sub> O <sub>3</sub>	C4 oxo-carboxylic acids	Acetic anhydride	CIMS and PTRMS
102.133	C <sub>5</sub> H <sub>10</sub> O <sub>2</sub>	C5 saturated carboxylic acids	Valeric acid	CIMS and PTRMS
114.144	C <sub>6</sub> H <sub>10</sub> O <sub>2</sub>	Sum of cyclic saturated and n-saturated C5 carboxylic acids	Caprolactone/c6 esters/c6diketone isomers	CIMS and PTRMS
116.16	C <sub>6</sub> H <sub>12</sub> O <sub>2</sub>	C6 carboxylic acids	Butyl acetate/c6 esters	CIMS and PTRMS
118.132	C <sub>7</sub> H <sub>10</sub> O <sub>2</sub>	Unsaturated C6 cyclic carboxylic acids	Cyclohexene carboxylic acid	CIMS and PTRMS
128.171	C <sub>7</sub> H <sub>12</sub> O <sub>2</sub>	C6 unsaturated carboxylic acids	Cyclohexanoic acid	CIMS and PTRMS
130.187	C <sub>7</sub> H <sub>14</sub> O <sub>2</sub>	C7 saturated carboxylic acids	Amyl acetate	CIMS and PTRMS

425

426

427 Table S6. Compounds with no significant observed emissions

<b>Molecular Weight</b>	<b>Formula</b>	<b>Compound Name</b>	<b>Instrument</b>
34.08	H <sub>2</sub> S	hydrogen sulfide	PTRMS
70.05	C <sub>2</sub> H <sub>3</sub> O <sub>2</sub>	Propiolic acid	PTRMS
72.17	C <sub>5</sub> H <sub>12</sub>	2,2-dimethylpropane	AWAS
82.06	C <sub>4</sub> H <sub>2</sub> O <sub>2</sub>	cyclobutenedione	PTRMS
85.06	C <sub>3</sub> H <sub>3</sub> NO <sub>2</sub>	cyanoacetic acid	CIMS
86.2	C <sub>6</sub> H <sub>14</sub>	2,2-dimethylbutane	AWAS
91.07	C <sub>2</sub> H <sub>5</sub> NO <sub>3</sub>	C2 nitro alcohol	CIMS
100.07	C <sub>4</sub> H <sub>4</sub> O <sub>3</sub>	dihydro furandione	PTRMS
102.195	C <sub>5</sub> H <sub>10</sub> S	cyclopentanethiol	PTRMS
104.105	C <sub>4</sub> H <sub>8</sub> O <sub>3</sub>	C4 hydroxy-carboxylic acids	CIMS
112.24	C <sub>8</sub> H <sub>16</sub>	cis-1,2-dimethylcyclohexane	AWAS
112.56	C <sub>6</sub> H <sub>5</sub> Cl	chlorobenzene	PTRMS
118.13	C <sub>5</sub> H <sub>10</sub> O <sub>3</sub>	C5 hydroxy-carboxylic acids	CIMS
128.29	C <sub>9</sub> H <sub>20</sub>	2,5-dimethylheptane	AWAS
134.24	C <sub>10</sub> H <sub>14</sub>	1-methyl-2-n-propylbenzene	AWAS
140.25	C <sub>8</sub> H <sub>12</sub> S	butylthiophene	PTRMS
142.32	C <sub>10</sub> H <sub>22</sub>	2,2-dimethyloctane	AWAS
147.00	C <sub>6</sub> H <sub>4</sub> Cl <sub>2</sub>	dichlorobenzene	PTRMS
154.12	C <sub>7</sub> H <sub>6</sub> O <sub>4</sub>	dihydroxybenzoic acid	PTRMS
n/a	Cl <sup>-</sup>	p-chloride	AMS

428

429

430

431

432

433

434

435

436

437

438

439

440

441 Table S7. Emission ratios (relative to CO, as  $\mu\text{g m}^{-3}$  of I/SVOC per  $\mu\text{g m}^{-3}$  CO) for complex mixtures of  
 442 gas-phase CH, CHO<sub>1</sub>, and CHS<sub>1</sub> compounds grouped by carbon number for all targeted molecular  
 443 formulas, derived from the integrated cartridge samples, using the sample taken across the lowest  
 444 transects of Screen 1. ~~Note: based on flight design, it was not possible to directly derive emission factors~~  
 445 ~~due to the lack of background cartridge samples in the upwind region of the fire so ratios to CO in the~~  
 446 ~~concentrated lower (Screen 1) transects are used in the analysis to approximate emission factors from the~~  
 447 ~~wildfire.~~The ERs are reported as a range with the lower limit reflecting the subtraction of a slightly  
 448 contaminated background, and the upper limit having no background subtracted.

Carbon Number	CH ( $\mu\text{g m}^{-3}$ )/ CO ( $\mu\text{g m}^{-3}$ )	CHO <sub>1</sub> ( $\mu\text{g m}^{-3}$ )/ CO ( $\mu\text{g m}^{-3}$ )	CHS <sub>1</sub> ( $\mu\text{g m}^{-3}$ )/ CO ( $\mu\text{g m}^{-3}$ )
10	1.1E-02 - 1.1E-02	3.2E-03 - 3.2E-03	7.2E-06 - 7.9E-06
11	0.0E+00 - 0.0E+00	6.6E-04 - 6.6E-04	1.6E-05 - 1.6E-05
12	5.4E-05 - 5.4E-05	4.6E-04 - 7.4E-04	0.0E+00 - 2.4E-06
13	3.3E-06 - 2.4E-04	4.4E-05 - 5.4E-04	9.2E-06 - 1.4E-05
14	5.3E-05 - 1.6E-04	3.7E-04 - 1.1E-03	4.4E-06 - 5.8E-06
15	6.0E-05 - 3.7E-04	3.3E-04 - 1.0E-03	2.2E-05 - 2.4E-05
16	3.4E-04 - 1.1E-03	3.6E-04 - 7.0E-04	5.4E-05 - 6.8E-05
17	7.6E-04 - 1.2E-03	1.2E-03 - 1.9E-03	3.3E-04 - 3.4E-04
18	1.0E-03 - 1.7E-03	2.1E-04 - 1.3E-03	1.2E-04 - 1.2E-04
19	1.6E-03 - 1.9E-03	5.7E-04 - 1.2E-03	3.9E-04 - 4.3E-04
20	1.9E-03 - 2.8E-03	3.1E-04 - 9.1E-04	1.1E-04 - 1.4E-04
21	2.5E-03 - 2.5E-03	2.6E-04 - 5.2E-04	2.3E-04 - 2.9E-04
22	3.8E-03 - 4.0E-03	1.7E-04 - 3.3E-04	1.9E-05 - 8.9E-05
23	2.1E-03 - 2.2E-03	6.7E-05 - 1.5E-04	2.9E-05 - 2.9E-05
24	7.6E-04 - 1.0E-03	3.3E-05 - 1.2E-04	4.4E-05 - 6.0E-05
25	4.0E-04 - 4.3E-04	9.0E-06 - 5.5E-05	1.3E-05 - 6.1E-05

449  
 450  
 451  
 452  
 453  
 454  
 455  
 456  
 457  
 458  
 459  
 460

461 Table S8. Compounds shown in Fig. 9 where the identifications/naming are not exact matches with  
 462 the current study. 1 Individually identified compounds were summed for comparison to the present study;  
 463 2 Each compound was compared with the value from the present study.

Molecular Weight	Compound	Instrument	Compound Name	Andreae Names	Koss Names	Permar Names	Urbanski Names
54.092	C <sub>4</sub> H <sub>6</sub>	PTRMS	butadiene/fr agments	butadiene	1,3-butadiene + 1,2- butadiene	1,3-butadiene, 1,2-butadiene	n/a
54.092	C <sub>4</sub> H <sub>6</sub>	AWAS	1,3- butadiene	butadiene	1,3-butadiene + 1,2- butadiene	1,3-butadiene, 1,2-butadiene	n/a
57.052	C <sub>2</sub> H <sub>3</sub> NO	CIMS	hydroxy acetonitrile	n/a	methyl isocyanate + hydroxyaceto nitrile	methyl isocyanate, hydroxyacetonitril e	n/a
58.124	C <sub>4</sub> H <sub>10</sub>	AWAS	isobutane	n/a	n/a	n-Butane	n/a
60.052	C <sub>2</sub> H <sub>4</sub> O <sub>2</sub>	CIMS	acetic acid	Acetic acid	acetic acid + glycolaldehyd e	acetic acid, glycolaldehyde (=hydroxyacetalde hyde)	n/a
60.096	C <sub>3</sub> H <sub>8</sub> O	PTRMS	propanol	n/a	n/a	Isopropanol	n/a
66.103	C <sub>5</sub> H <sub>6</sub>	PTRMS	cyclopentan diene	n/a	n/a	1,3- cyclopentadiene	1,3- Cyclopentadie nePIT
70.091	C <sub>4</sub> H <sub>6</sub> O	PTRMS	MVK, methacrolein , crotonaldehy de	Methacrolei n	MVK + methacrolein + crotonaldehy de	Methyl vinyl ketone, Methacrolein, 2- Butenal (=crotonaldehyde)	<sup>1</sup> Crotonaldehy de + Methacrolein + Methyl Vinyl Ketone MVK
70.135	C <sub>5</sub> H <sub>10</sub>	PTRMS	pentene/met hyl butene/frag ments	1-Pentene + 2-pentene	pentene+met hyl butene	pentenes, methylbutenes	n/a
70.135	C <sub>5</sub> H <sub>10</sub>	AWAS	c-2-pentene	2 pentene cis&tran	pentene+met hyl butene	pentenes, methylbutenes	n/a
70.135	C <sub>5</sub> H <sub>10</sub>	AWAS	cyclopentan e			cyclopentane	n/a
70.135	C <sub>5</sub> H <sub>10</sub>	AWAS	1-pentene	1-Pentene	pentene+met hyl butene	pentenes, methylbutenes	n/a
70.135	C <sub>5</sub> H <sub>10</sub>	AWAS	methyl-1- butene	1-Pentene	pentene+met hyl butene	pentenes, methylbutenes	n/a
70.135	C <sub>5</sub> H <sub>10</sub>	AWAS	methyl-2- butene	1-Pentene	pentene+met hyl butene	pentenes, methylbutenes	n/a
72.063	C <sub>3</sub> H <sub>4</sub> O <sub>2</sub>	CIMS	acrylic acid	n/a	n/a	pyruvaldehyde (=methyl glyoxal), acrylic acid	n/a
72.107	C <sub>4</sub> H <sub>8</sub> O	PTRMS	methyl ethyl ketone + butanal + 2- methylpropan al	2-butanone (methyl ethyl ketone)	methyl ethyl ketone + butanal + 2- methylpropan al	methyl ethyl ketone, 2- methylpropanal, butanal	<sup>1</sup> Methyl Ethyl Ketone MEK + n-Butanal + 2-

							Methylpropanal
72.151	C <sub>5</sub> H <sub>12</sub>	AWAS	methylbutane	n/a	n/a	n-pentane	n/a
74.079	C <sub>3</sub> H <sub>6</sub> O <sub>2</sub>	PTRMS	hydroxy acetone/ethyl formate	n/a	methyl acetate + ethyl formate + hydroxyacetone	Hydroxyacetone, Methyl acetate, Ethyl formate	Ethyl Formate
81.118	C <sub>5</sub> H <sub>7</sub> N	PTRMS	pentene nitriles/methyl pyrrole	n/a	n/a	n/a	1-Methylpyrrole
82.102	C <sub>5</sub> H <sub>6</sub> O	PTRMS	methyl furan	n/a	2-methylfuran + 3-methylfuran + general HCO	2-Methylfuran, 3-Methylfuran	<sup>2</sup> 2-Methylfuran, 3-Methylfuran
84.118	C <sub>5</sub> H <sub>8</sub> O	PTRMS	cyclopentanone/ isomers	n/a	3-methyl-3-butene-2-one + cyclopentanone + HCO1 isomers	3-Methyl-3-buten-2-one, Cyclopentanone	Cyclopentanone
84.162	C <sub>6</sub> H <sub>12</sub>	PTRMS	hexene/fragments	1-hexene	n/a	n/a	<sup>2</sup> 1-Hexene, cis-2-Hexene
86.09	C <sub>4</sub> H <sub>6</sub> O <sub>2</sub>	PTRMS	butanedione/ isomers	2,3-butanedione	2,3-butanedione + methyl acrylate + other HCO2	2,3-butanedione, methyl acrylate	2,3-Butadione
86.134	C <sub>5</sub> H <sub>10</sub> O	PTRMS	pentanone	n/a	n/a	n/a	<sup>2</sup> 2-Pentanone, 3-Pentanone
86.178	C <sub>6</sub> H <sub>14</sub>	AWAS	2+,3-methylpentane	n/a	n/a	3-methylpentane	3-Methylpentane
96.085	C <sub>5</sub> H <sub>4</sub> O <sub>2</sub>	PTRMS	furfural	furfural (2-furaldehyde)	2-furfural + 3-furfural + other HCO2	2-furfural (=furaldehyde), 3-furfural	2-Furaldehyde
98.189	C <sub>7</sub> H <sub>14</sub>	PTRMS	heptene	n/a	n/a	n/a	1-Heptene
100.117	C <sub>5</sub> H <sub>8</sub> O <sub>2</sub>	PTRMS	methyl methacrylate / isomers	n/a	Methyl methacrylate + other HCO2	Methyl methacrylate	Methyl Methacrylate
100.161	C <sub>6</sub> H <sub>12</sub> O	PTRMS	hexanal/hexanones	n/a	hexanal + hexanones	Hexanones, Hexanal	<sup>1</sup> n-Hexanal + Hexanones
103.124	C <sub>7</sub> H <sub>5</sub> N	PTRMS	benzonitrile	n/a	Benzonitrile	Benzonitrile	Benzenenitrile
106.168	C <sub>8</sub> H <sub>10</sub>	PTRMS	C8 aromatics	n/a	Ethyl benzene + m-xylene + p-	C8 Aromatics	<sup>1</sup> Ethylbenzene + m,p-Xylenes + o-Xylene

					xylene + o-xylene		
112.216	C <sub>8</sub> H <sub>16</sub>	PTRMS	octene	n/a	n/a	n/a	1-Octene
118.135	C <sub>8</sub> H <sub>6</sub> O	PTRMS	benzofuran	n/a	Benzofuran	Benzofuran	BenzofuranPI T
118.179	C <sub>9</sub> H <sub>10</sub>	PTRMS	methylstyrenes/ propenyl benzenes	n/a	Indane + methyl styrenes + propenyl benzenes	Methylstyrenes, Indane, Propenylbenzenes	<sup>1</sup> 1-Propenylbenzene, 2-Methylstyrene, 2-Propenylbenzene, 3-Methylstyrene, 4-Methylstyrene, alpha-Methylstyrene
120.195	C <sub>9</sub> H	PTRMS	C9 aromatics	1,2,3-trimethylbenzene, 1,2,4-trimethylbenzene, 1,3,5-trimethylbenzene (Simpson et al., 2011)	C9 aromatics	C9 aromatics	<sup>1</sup> 1,2,3-Trimethylbenzene, 1,2,4-Trimethylbenzene, 1,3,5-Trimethylbenzene, 1-Ethyl-2-Methylbenzene, 1-Ethyl-3,4-Methylbenzene, Isopropylbenzene, n-Propylbenzene
132.162	C <sub>9</sub> H <sub>8</sub> O	PTRMS	methyl benzo furans	n/a	Methyl benzofuran	Methylbenzofurans	<sup>1</sup> Methylbenzofuran isomer 1, Methylbenzofuran isomer 2, Methylbenzofuran isomer 3
132.206	C <sub>10</sub> H <sub>12</sub>	PTRMS	ethyl styrene/ methyl propenyl benzene	n/a	Methyl propenyl benzene + ethyl styrene	Ethyl styrenes, Methylpropenylbenzenes, Butenylbenzenes	<sup>1</sup> 1-Methyl-1-Propenylbenzene, Ethylstyrene
134.222	C <sub>10</sub> H <sub>14</sub>	PTRMS	C10 Aromatics	n/a	C10 Aromatics	C10 Aromatics	<sup>1</sup> 1,4-Diethylbenzene,

							1-Butenylbenzene, Ethyl Xylene isomer 1, Ethyl Xylene isomer 2, Isobutylbenzene, Methyl-n-Propylbenzene isomer 1, Methyl-n-Propylbenzene isomer 2, n-Butylbenzene, p-Cymene
136.238	C <sub>10</sub> H <sub>16</sub>	PTRMS	monoterpenes	sum of alpha + beta-pinene (Simpson et al., 2011)	monoterpenes	monoterpenes	n/a
148.249	C <sub>11</sub> H <sub>16</sub>	PTRMS	C11 aromatics/pentamethyl benzene	n/a	n/a	n/a	C11 Aromatics

464

465

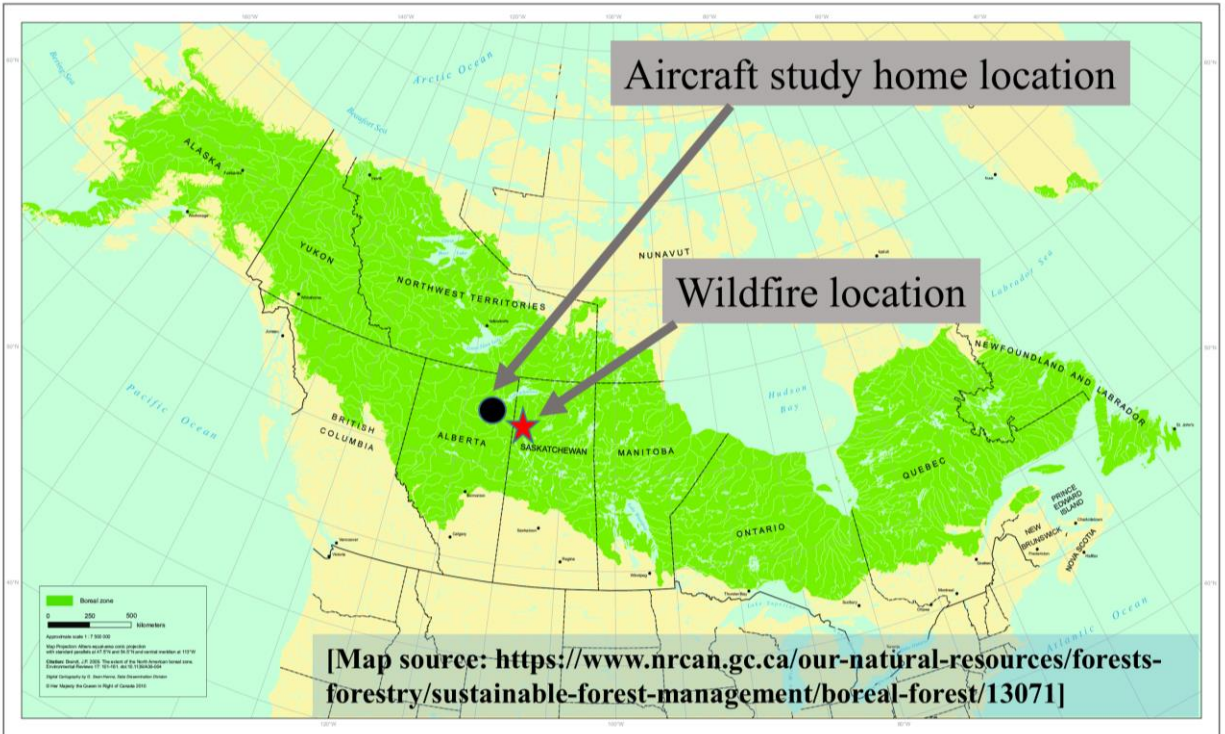
466 Table S9. Emission speciation profile for SAPRC11 chemical mechanism derived from normalized EFs  
 467 from the present study and compared with wildfire smoldering emission speciation profile from the EPA  
 468 SPECIATEv4.5 #95428 dataset. Note that SESQ (sesquiterpene), WSOC (water soluble organic carbon)  
 469 and IVOC are non-standard SAPRC11 mechanism species. Please refer to Carter and Heo (2013) for  
 470 mechanism species definition.

<b>SAPRC11 Lumped Species Name</b>	<b>Molecular Weight (g/mol)</b>	<b>Normalized Mass Fraction (Hayden et al.)</b>	<b>Normalized Mass Fraction (SPECIATEv4.5 #95428)</b>
CCOOH	60.05	0.038	0.031
ACET	58.08	0.024	0.0072
ACYL	26.04	0.0080	0.00059
ALK1	30.07	0.039	0.011
ALK2	36.73	0.013	0.0043
ALK3	58.61	0.0063	0.0077
ALK4	77.6	0.0055	0.030
ALK5	118.89	0.0053	0.28
ARO1	95.16	0.031	0.034
ARO2	118.72	0.042	0.067
BACL	86.09	0.021	0.0050
BALD	106.13	0.0020	0.0034
BENZ	78.11	0.013	0.0035
CATL	110.1	0.0032	0.014
CCHO	44.05	0.032	0.023
CH4	16.043	0.24	0.044
CRES	108.14	0.0026	0.0027
ETHE	28.05	0.044	0.0065
HCOOH	46.03	0.0050	0.0038
GLY			0.000046
HCHO	30.03	0.030	0.0084
IPRD	100.12	0.00020	0.0037
ISOP	68.12	0.021	0.00041
MACR	70.09	0.010	0.0044
MEK	72.11	0.0066	0.0028
MEOH	32.04	0.057	0.016
MGLY			0.000037
MVK	70.09	0.0057	0.019
NROG	1	0.11	0.13
NVOL	1	1.18E-05	
OLE1	72.34	0.079	0.049
OLE2	75.78	0.019	0.025
PACD	74.08	0.055	0.00047
PHEN	94.11	0.0055	0.0054
PROD2	116.16	0.0044	0.027

RCHO	58.08	0.038	0.0035
TERP	136.24	0.024	0.032
XYNL	122.16	0.0080	
SESQ	204.35	0.039	
WSOC	227	0.013	
IVOC	227.3	0.0063	

471

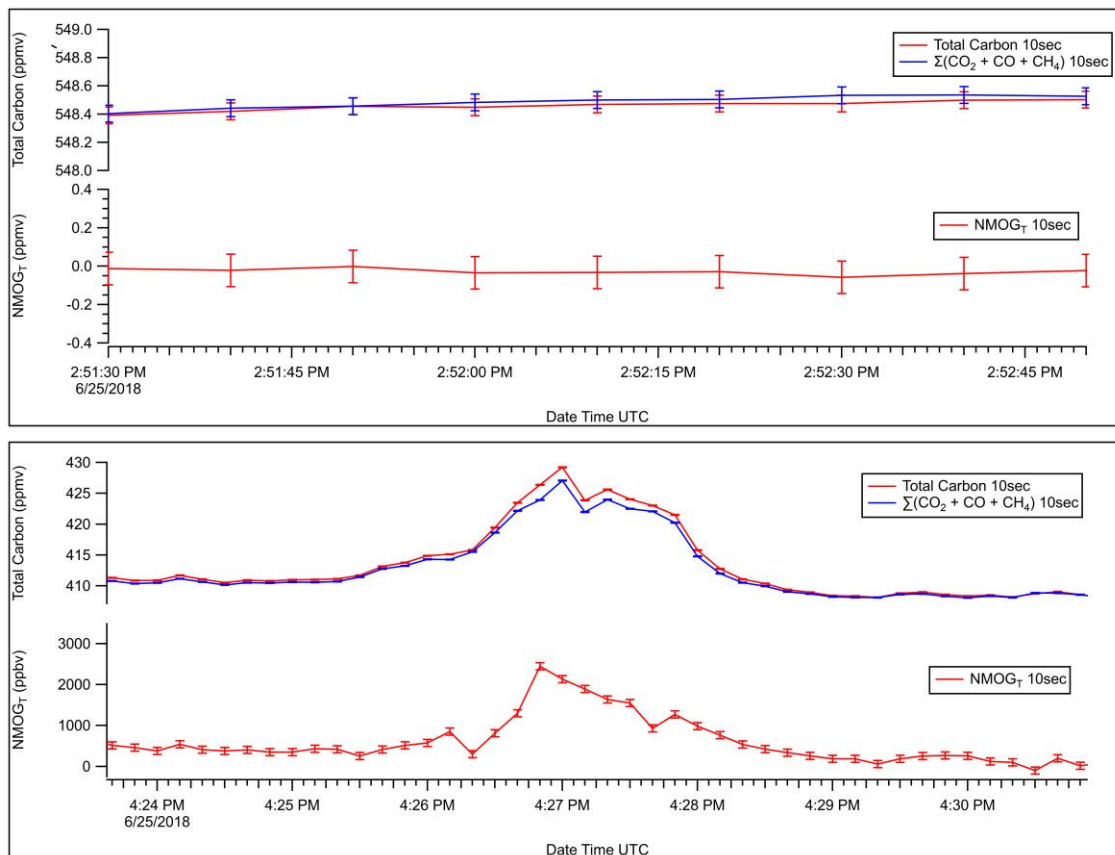
472



473

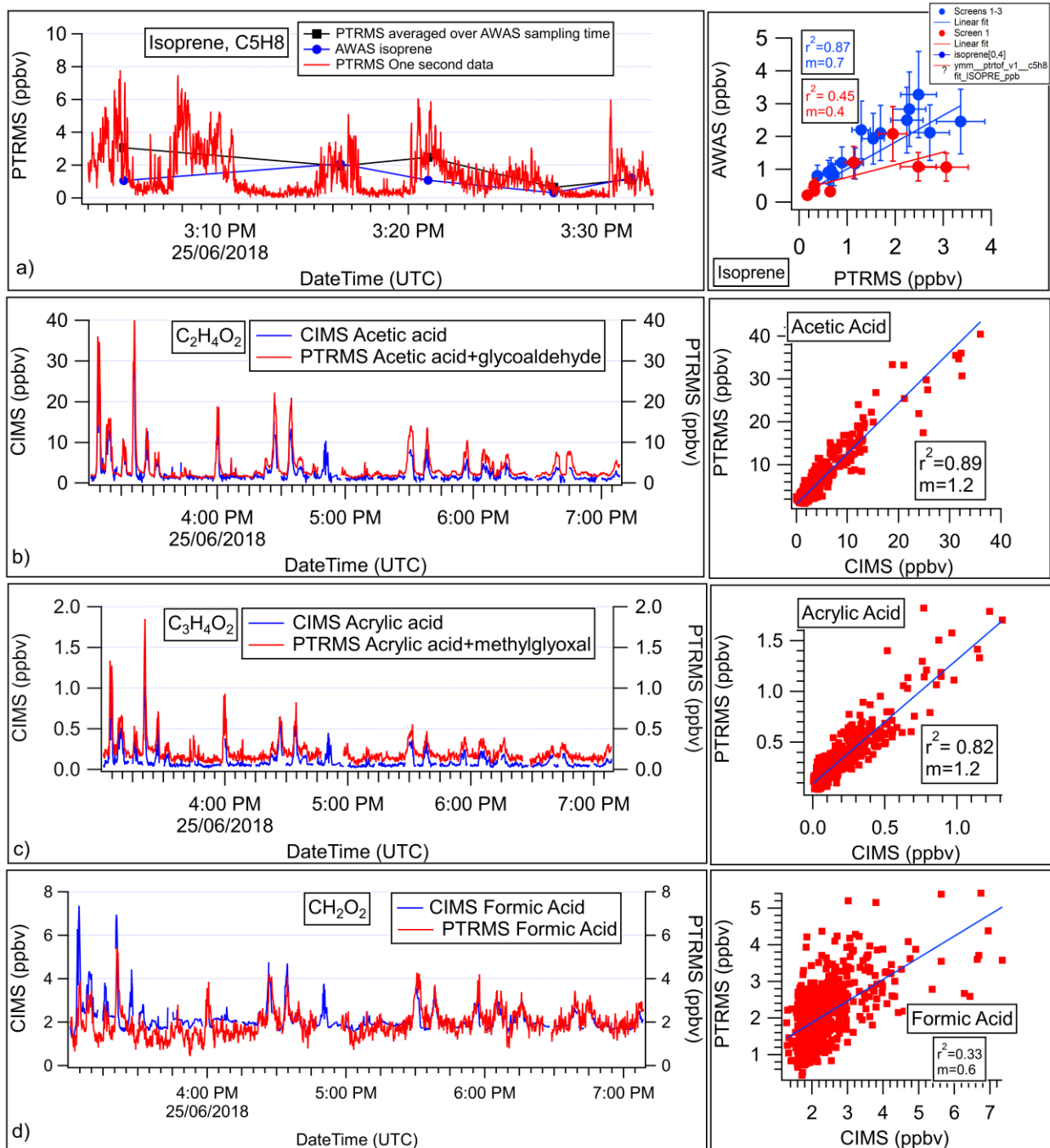
474 Figure S1. Map showing the home location of the airborne study at Fort McMurray, Alberta and the  
 475 location of the wildfire in Saskatchewan. The green shaded region shows the extent of the boreal forest  
 476 coverage across Canada and Alaska.

477



478  
 479 Figure S2. Total carbon (TC),  $\Sigma(\text{CO}_2+\text{CO}+\text{CH}_4)$  (ppmv C), and  $\text{NMOG}_T$  (ppmv C or ppbv C) averaged to  
 480 10 sec for a) a portion of the in-flight calibration time period, and b) a selected plume along Screen  
 481 1.  $\text{NMOG}_T$ , the difference between the TC and  $\Sigma(\text{CO}_2+\text{CO}+\text{CH}_4)$ , has an uncertainty of  $\pm 85$  ppbv C.

482  
 483  
 484  
 485  
 486  
 487  
 488  
 489  
 490  
 491  
 492  
 493



494

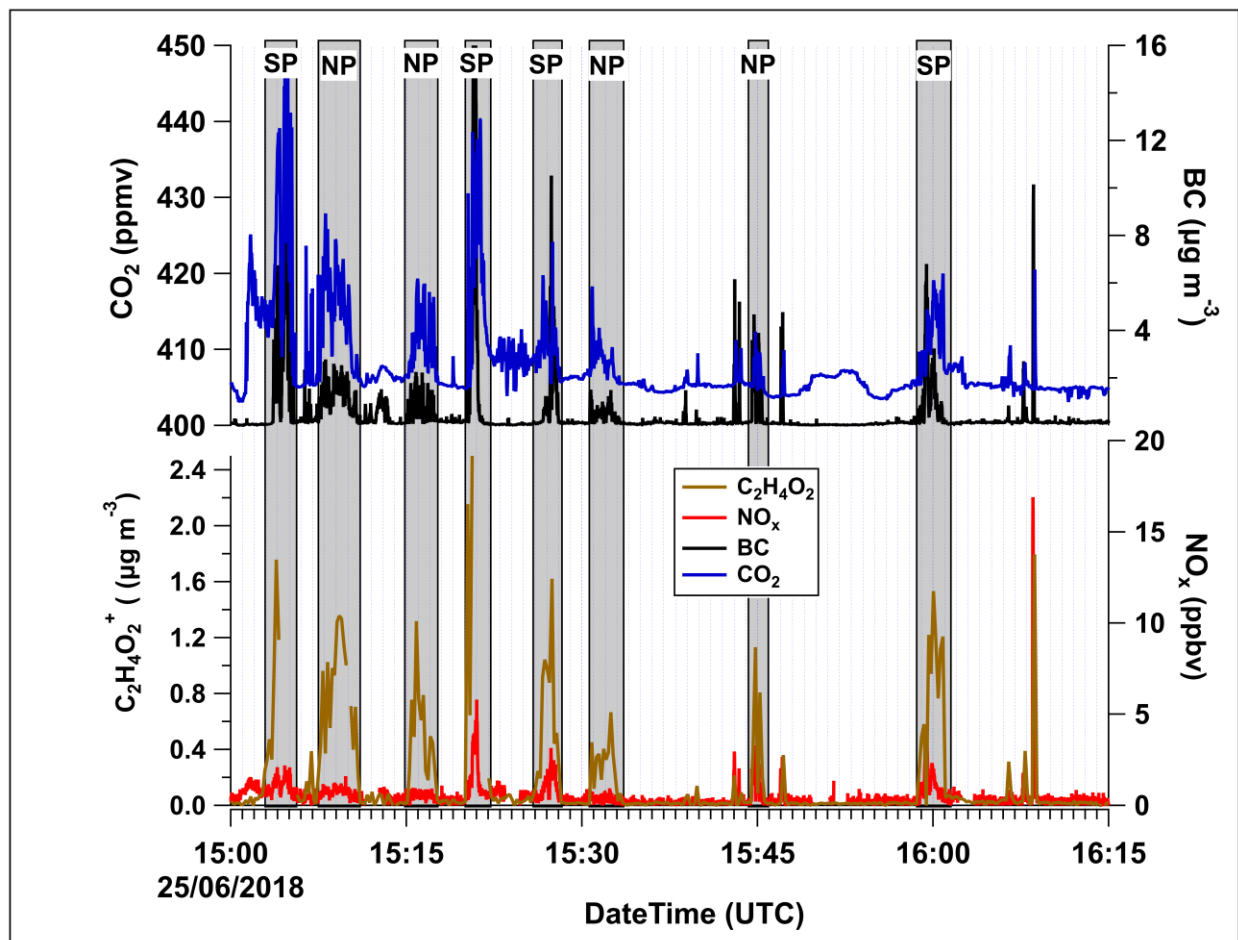
495 Figure S3. Intercomparisons of overlapping compounds between the PTRMS and AWAS, and between  
 496 the PTRMS and CIMS for a) isoprene, b) acetic acid, c) acrylic acid, and d) formic acid.

497

498

499

500



501

502 Figure S42. Time series of CO<sub>2</sub>, BC and NO<sub>x</sub> mixing ratios, and C<sub>2</sub>H<sub>4</sub>O<sub>2</sub><sup>+</sup> (levoglucosan fragment derived  
 503 from the AMS) concentrations for Screen 1. The in-plume portions are indicated by the vertical grey  
 504 bars. The aircraft flew back and forth across the plumes at increasing altitudes to complete five transects;  
 505 a transect represents one pass across the SP and NP at the same altitude.

506

507

508

509

510

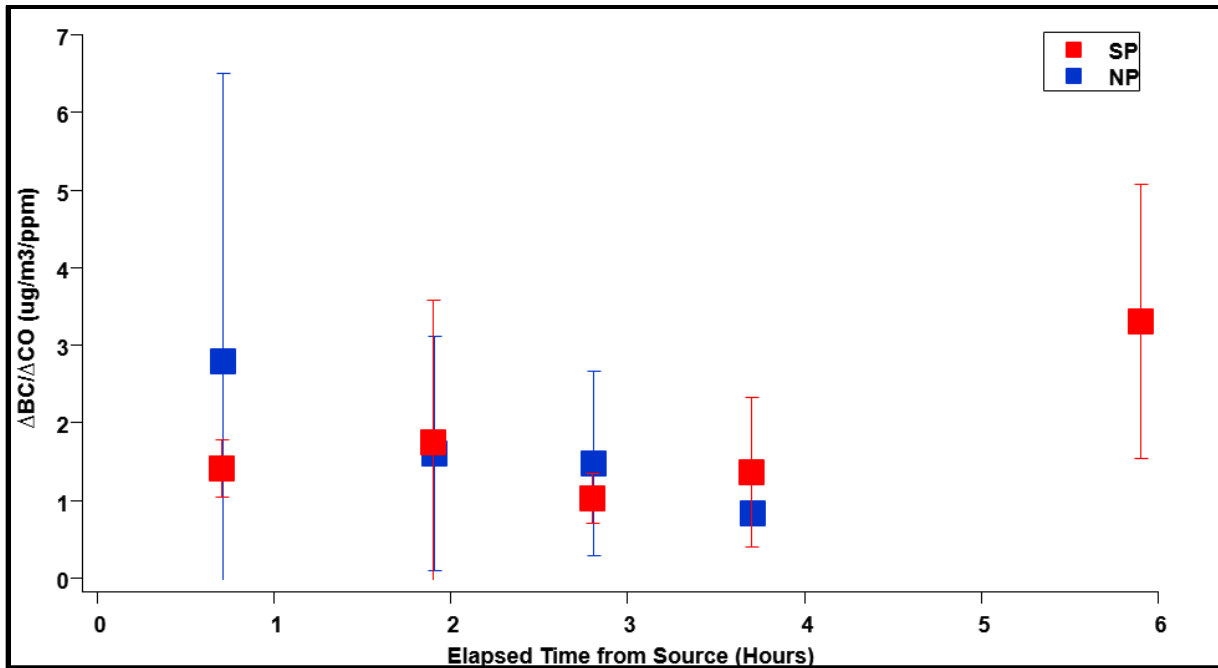
511

512

513

514

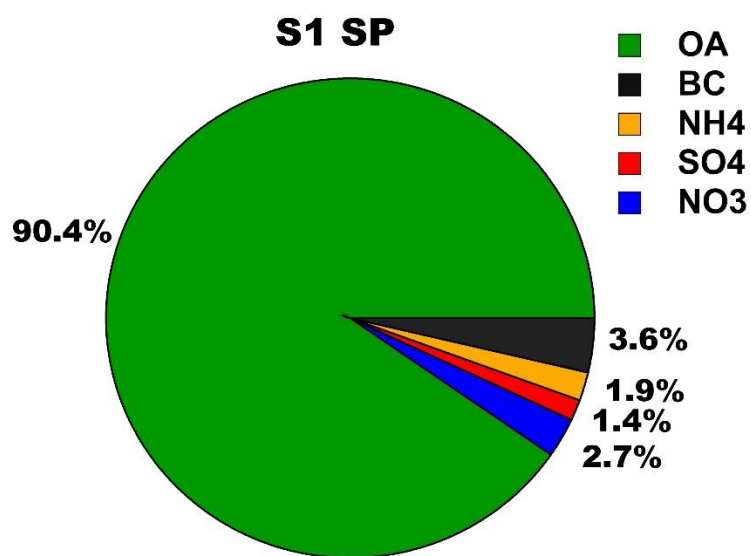
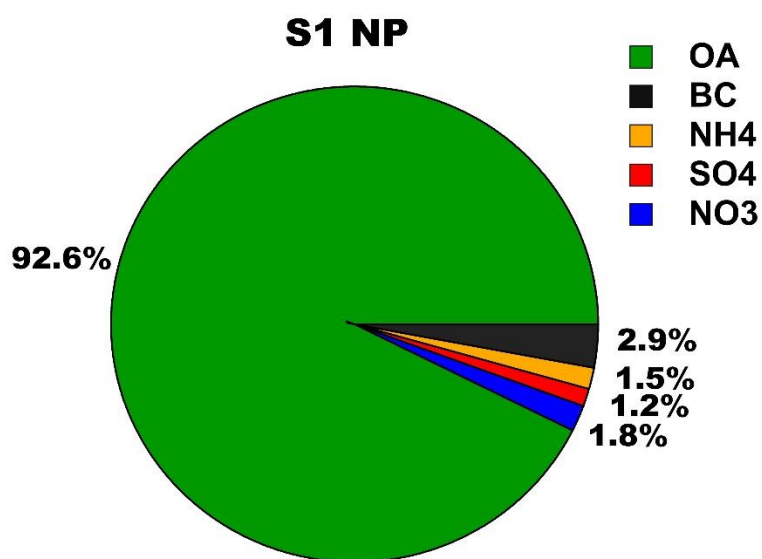
515



516

517 Figure S53. Using  $\Delta BC/\Delta CO$  (Selimovic et al., 2019) as an indicator of plume mixing downwind of the  
 518 Lac LaLoche fire. The squares show the average and the vertical lines the standard deviation for the  
 519 transects within the mixed layer for each screen.

520

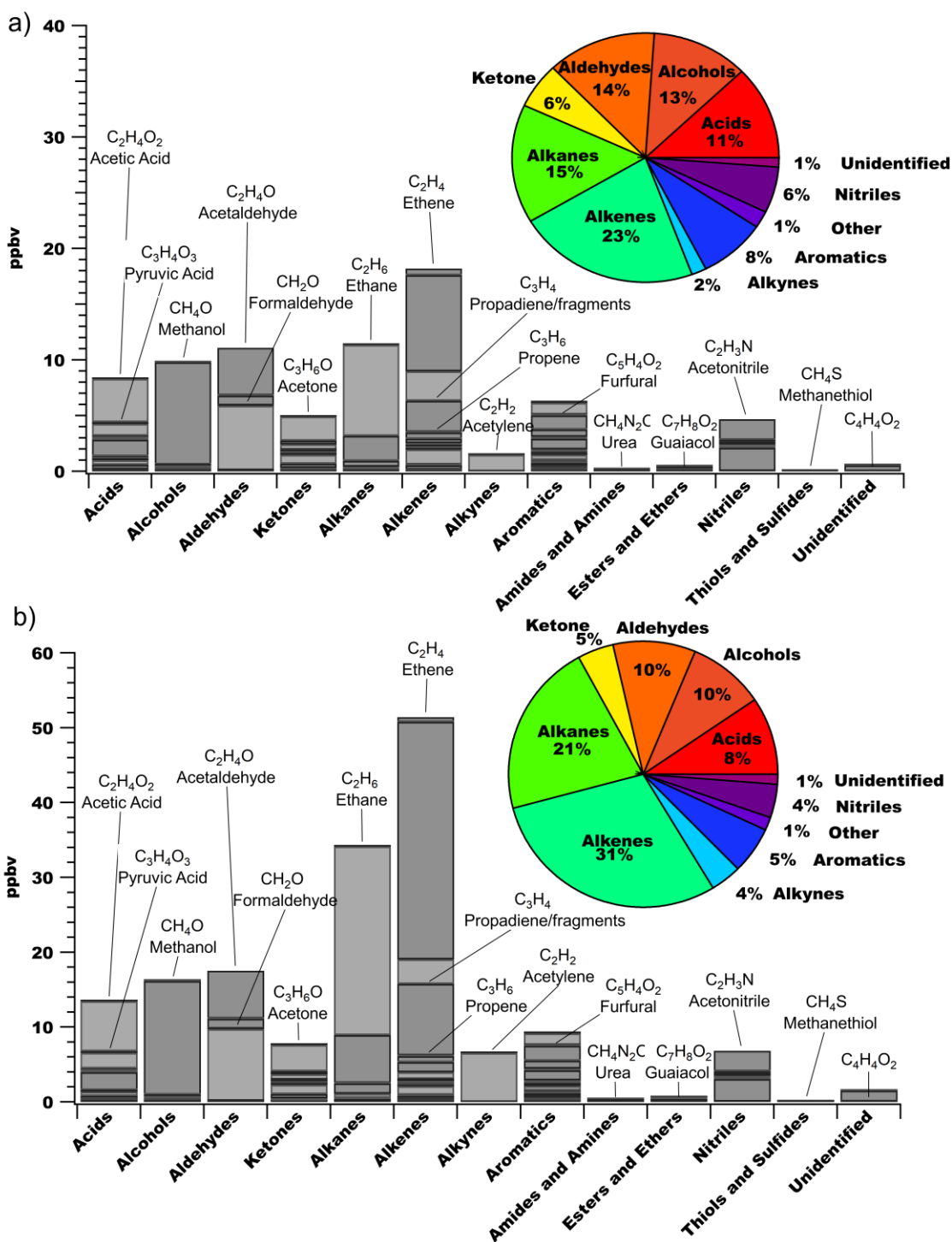


521

522 Figure S64. Percent contribution from individually measured particle-phase species for the NP and SP  
 523 including p-organics (OA), black carbon (BC), ammonium (NH<sub>4</sub>), sulphate (SO<sub>4</sub>) and nitrate (NO<sub>3</sub>), based  
 524 on mass concentrations.

525

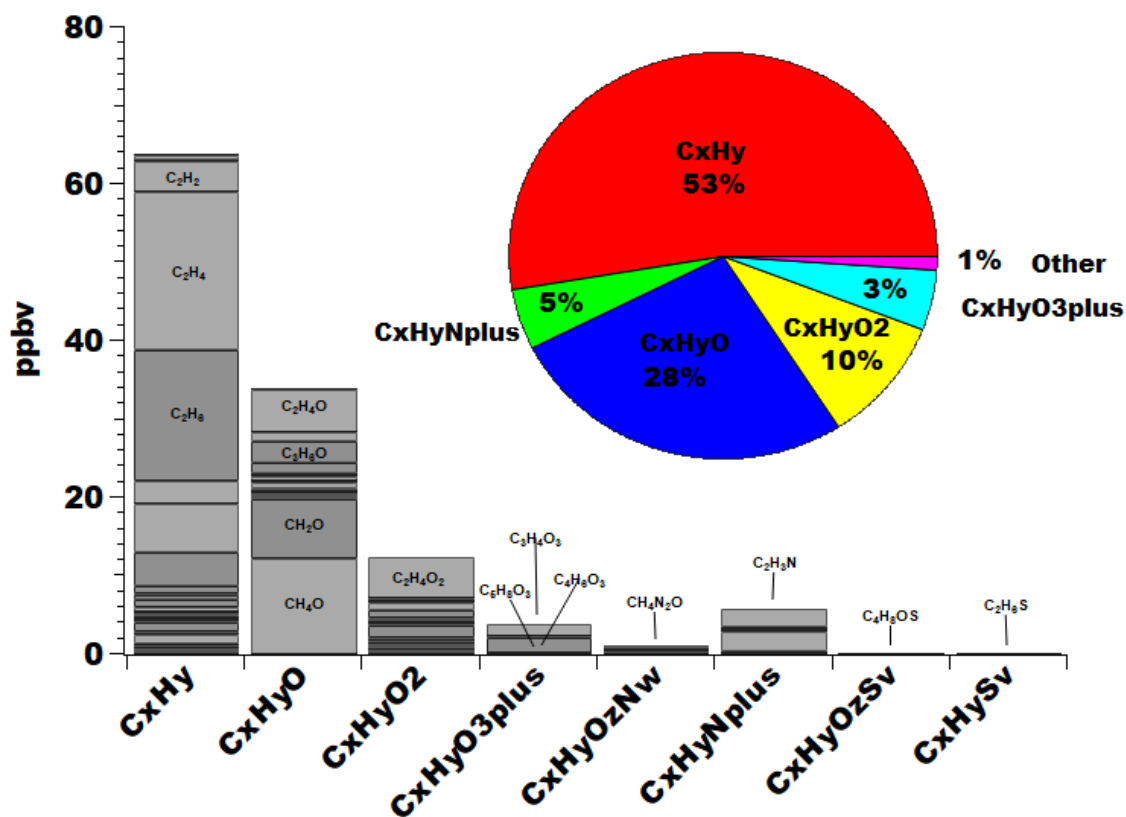
526



527

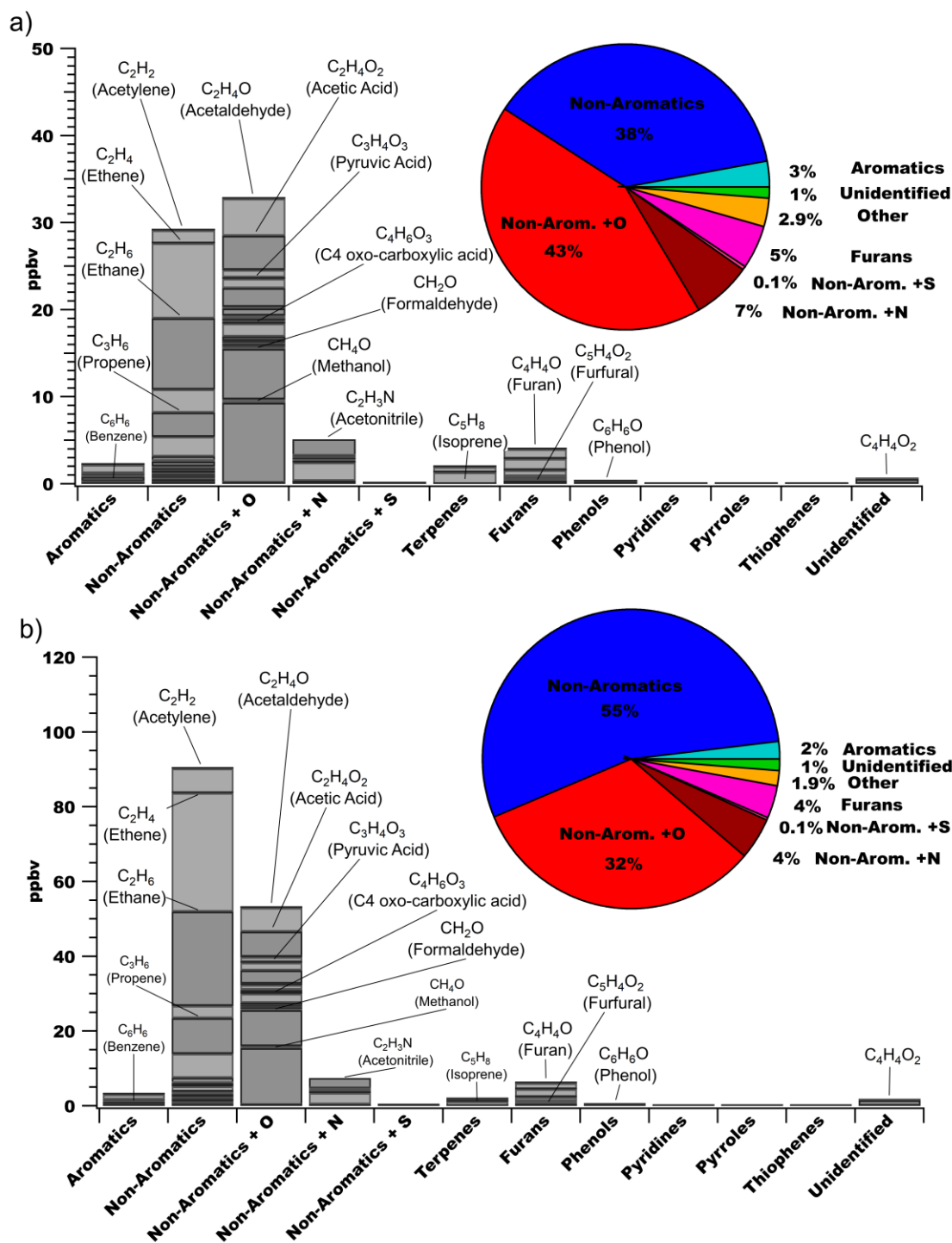
528 Figure S75. Background-subtracted mixing ratios of individually measured NMOGs from the PTRMS,  
 529 CIMS and AWAS are shown for thirteen chemical classes for the a) NP and b) SP. In some cases,  
 530 compounds are double- (or triple-) counted if they can be identified in more than one category. For  
 531 example, phenol is an alcohol + an aromatic; guaiacol is an alcohol + an ether + an aromatic. In the pie

532 chart, the *Other* category includes amides, amines, ethers, thiols and sulfides. The *Unidentified* category  
 533 contains molecular formulas detected but the compound(s) could not be identified.



534  
 535 Figure S86. Background-subtracted average mixing ratios of individually measured NMOGs from the  
 536 PTRMS, CIMS and AWAS are shown for molecular formulae classes. The *Unidentified* category  
 537 contains molecular formulas detected but the compound(s) could not be identified.

538

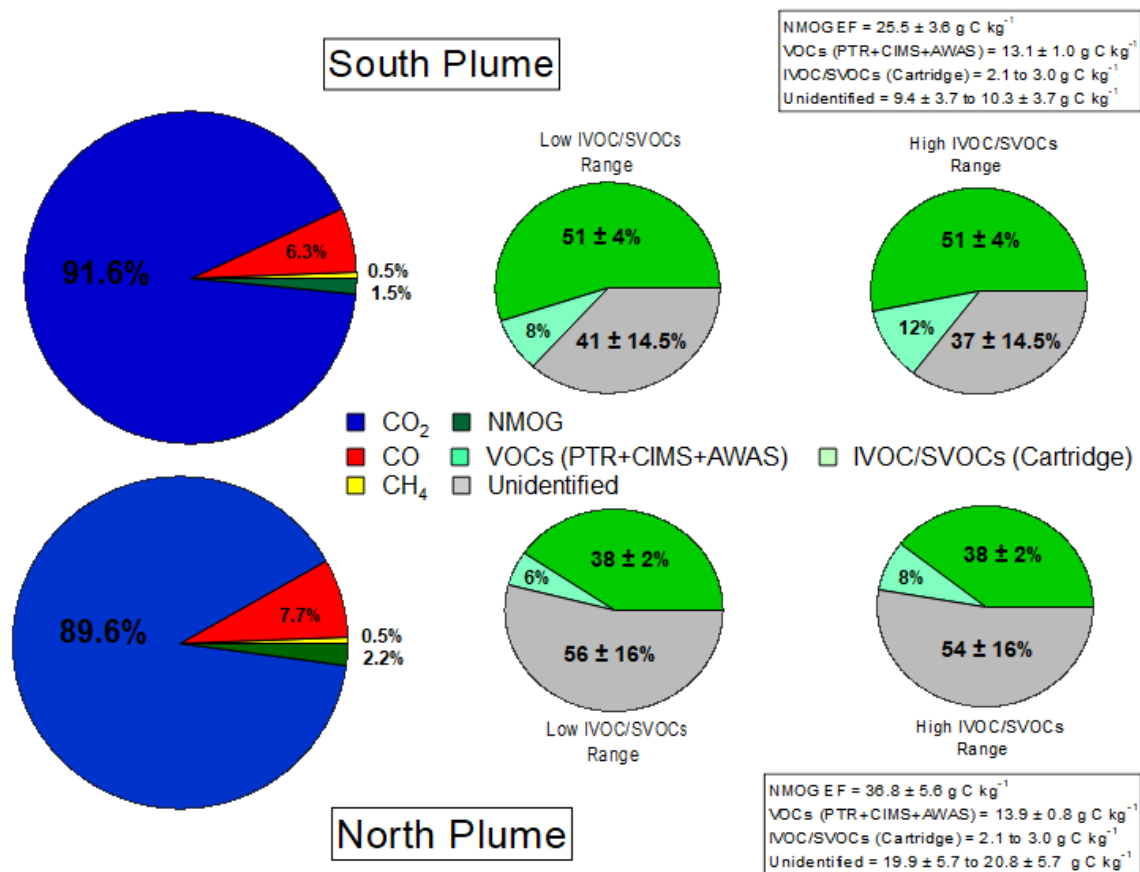


539

540 Figure S97. Average mixing ratios of individually measured NMOGs from the PTRMS, CIMS and  
 541 AWAS by structural group for the a) NP and b) SP. The *Other* category is the sum of terpenes, phenols,  
 542 pyridines, pyrroles and thiophenes.

543

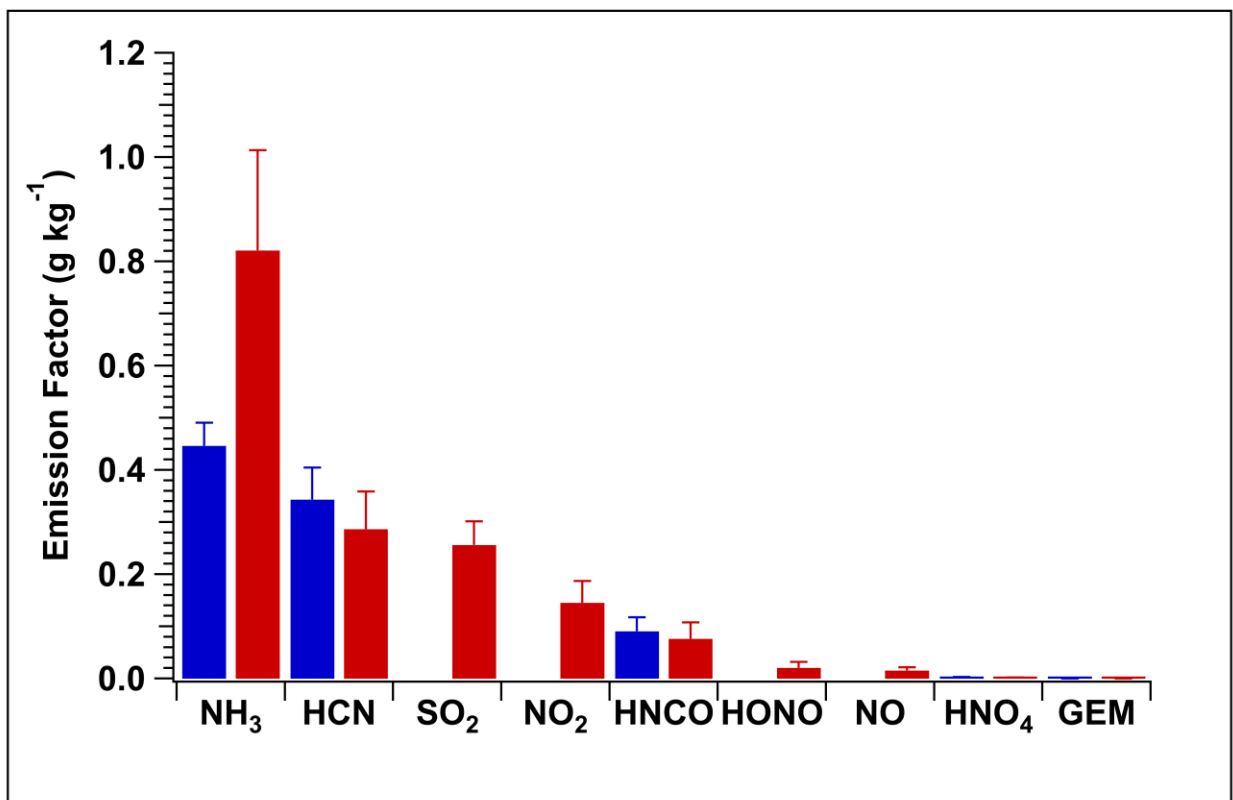
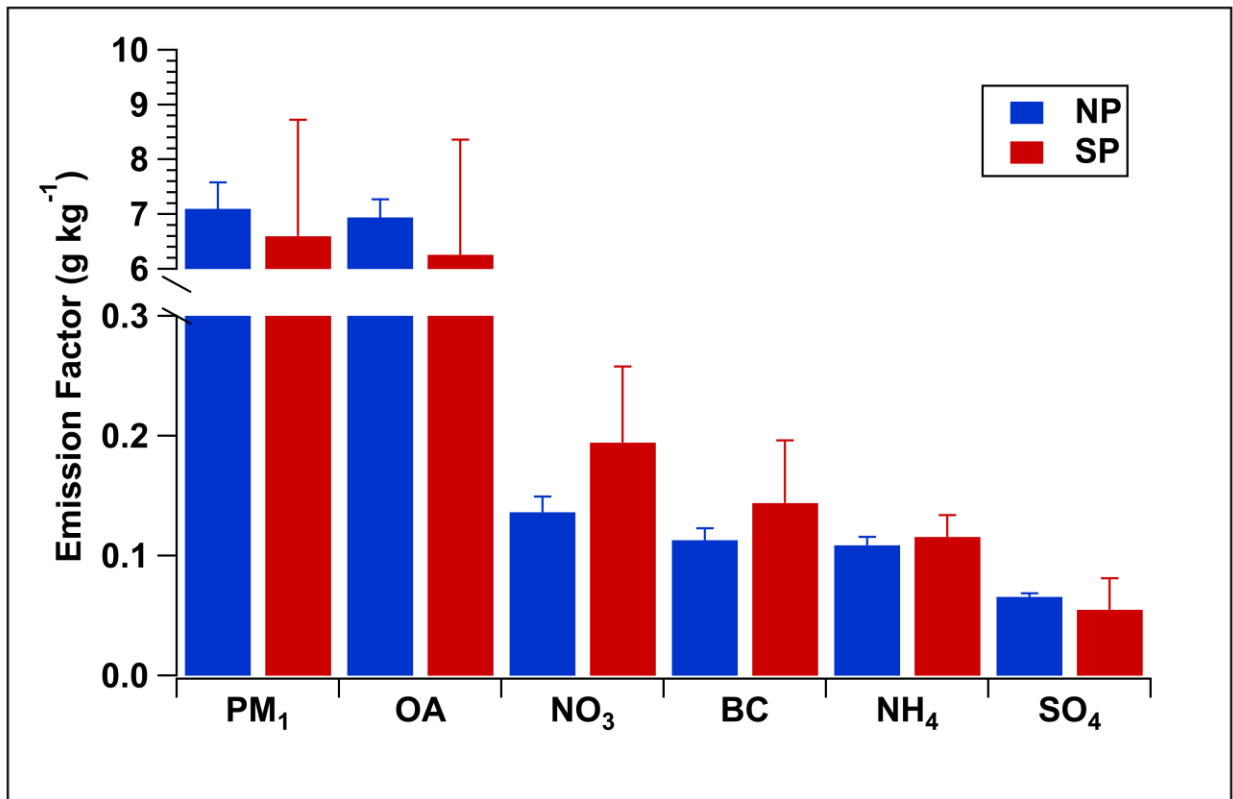
544



545

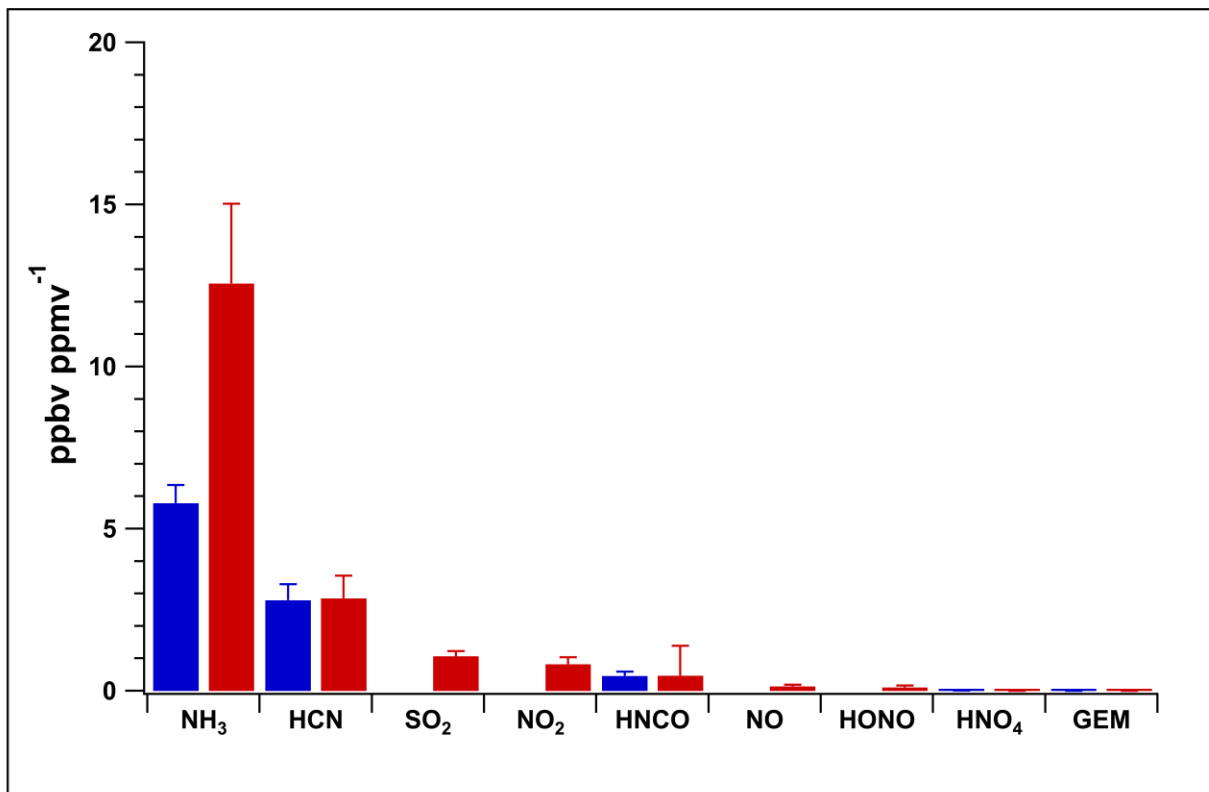
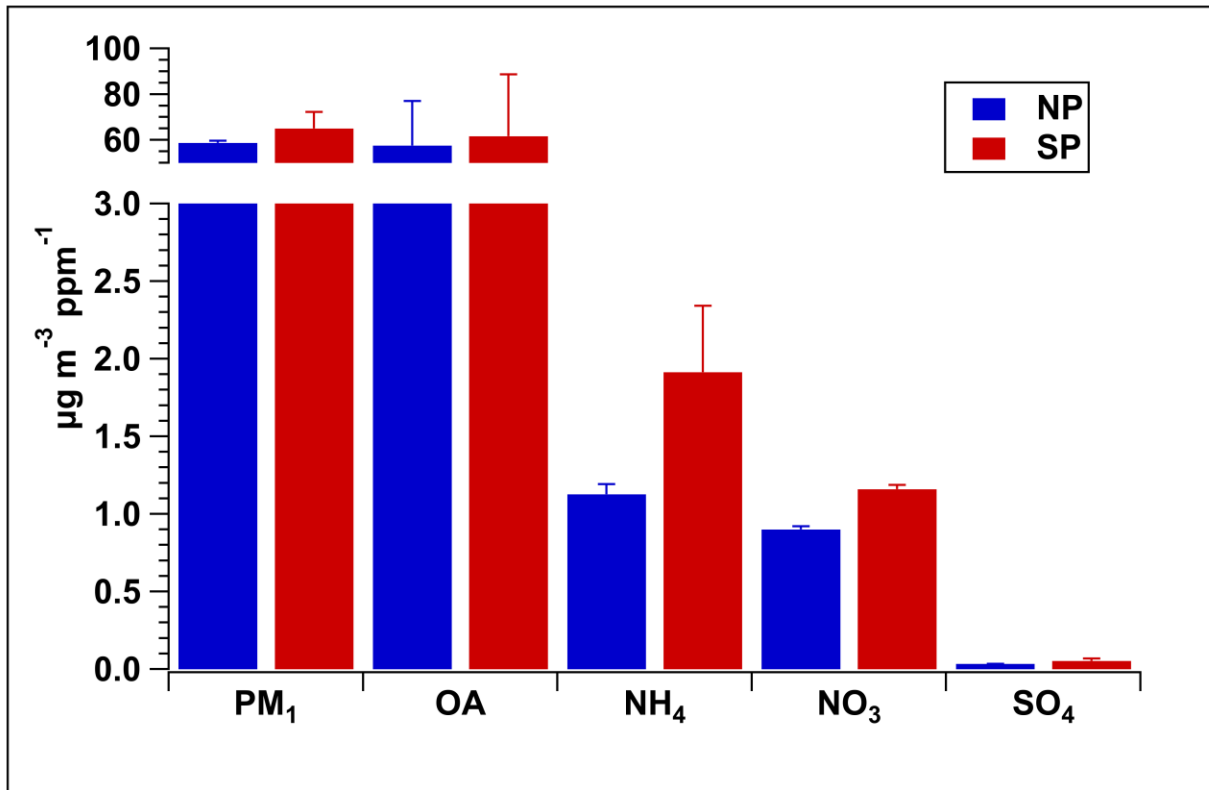
546 Figure S108. Percent contributions of carbon-containing compounds to the TC based on EFs (in terms of  
 547 carbon fraction) for the SP and NP. The two pie charts on the right, representing the low and high  
 548 I/SVOC EF estimates, -show the percent breakdown of the measured NMOGs and the remaining  
 549 unidentified portion. The EF values (g C kg<sup>-1</sup>) are identified in the boxes. Note, the I/SVOC  
 550 measurements represent the integrated average encompassing both plumes.

551



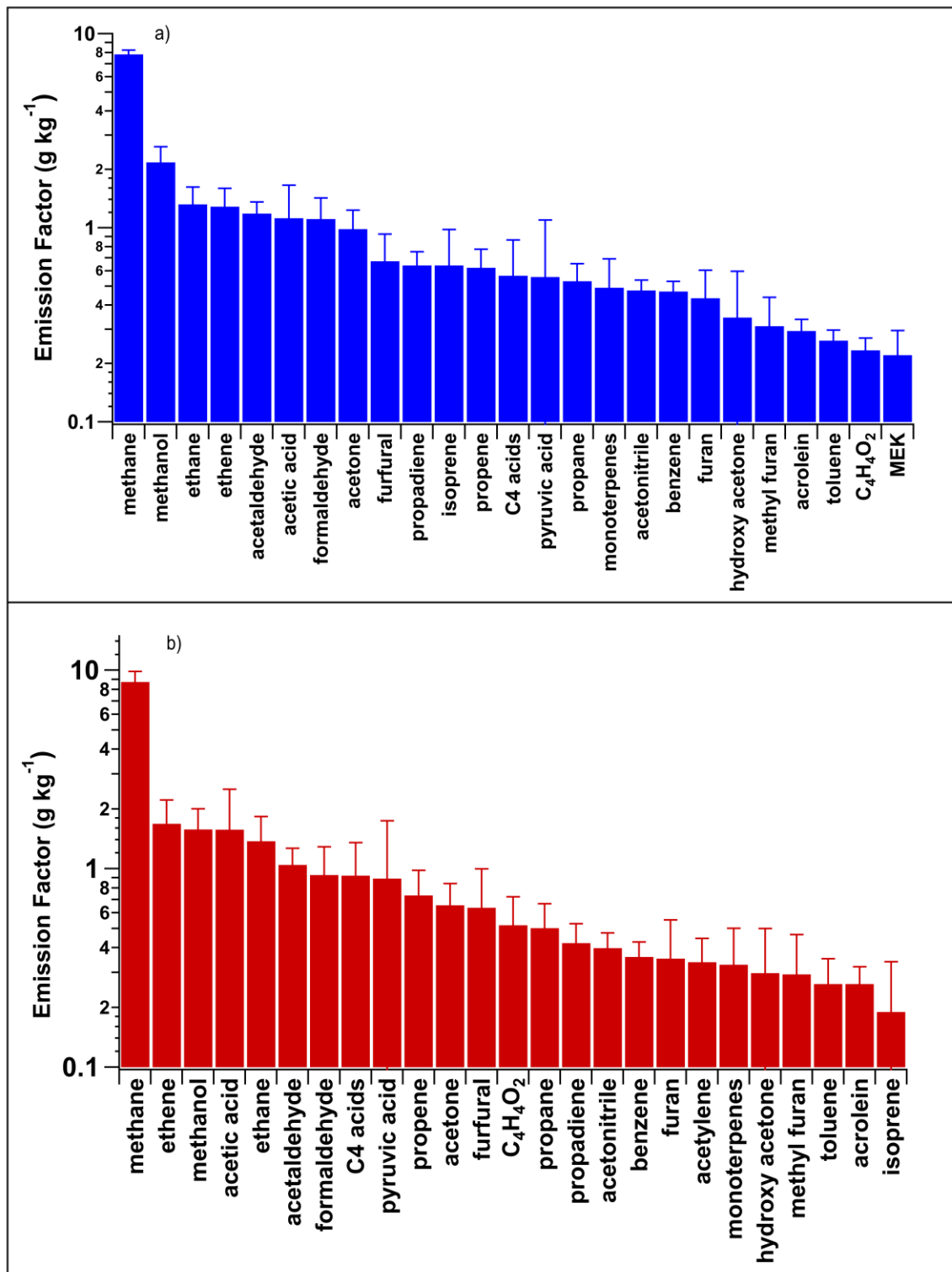
552

553 Figure S119. Emission factors (EF) (g kg<sup>-1</sup>) for the SP and NP determined from measurements of a)  
 554 particle species; and b) inorganic gas-phase species.



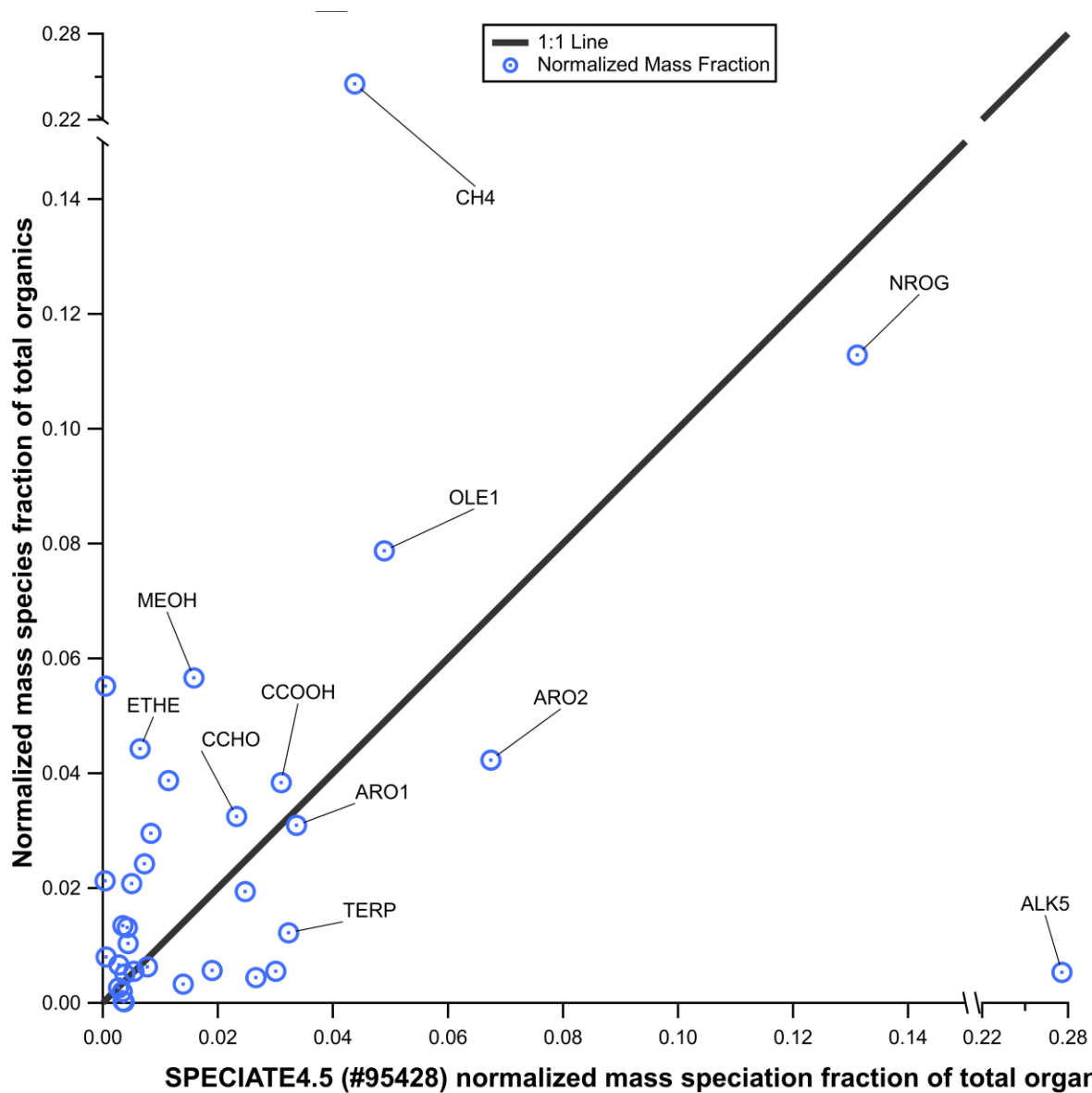
555

556 Figure S120. Emission ratios (ER) for the SP and NP determined from measurements of a) particle  
 557 species ( $\mu\text{g m}^{-3} \text{ppm}^{-1}$ ); and b) inorganic gas-phase species ( $\text{ppbv ppm}^{-1}$ ).



558

559 Figure S134. Emission factors (EF) (g kg<sup>-1</sup>) for the a) NP and b) SP for the top 25 measured gas-phase  
 560 organic species. ~~C5 acids = C5 oxo-carboxylic acids~~, C4 acids = C4 oxo-carboxylic acids, propadiene =  
 561 fragments/propadiene, hydroxy acetone = hydroxy acetone/ ethyl formate; MEK = MEK, butanal and 2-  
 562 methylpropanal .  
 563



564

565 Figure S142. Comparison of the **normalized** organic gas speciation profile **derived** from this study  
 566 (**Hayden et al.**) with that from the EPA's SPECIATE4.5 (#95428) profile. **used by the SAPRC-11**  
 567 **mechanism (SPECIATE4.5#95428).** EFs in the present study were mapped to the SAPRC-11 model  
 568 mechanism species and normalized to **the NMOG, total organic gas** (which **does not includes** the  
 569 unidentified mass fraction), to create **the a** total organic gas mass speciation profile. The **normalized**  
 570 **model species fraction total organic mass speciation profile** is plotted against the similarly treated mass  
 571 speciation profile from the EPA SPECIATEv4.5 #95428 for wildfire smoldering emissions. Note that for  
 572 comparison purposes the non-standard SAPRC-11 species in the present study are lumped, such that  
 573 SESQ is summed with TERP, and IVOC, WSOC and NVOL are summed with NROG.

574

575

576

577

578

579 **References**

580 Akagi, S. K., Yokelson, R. J., Wiedinmyer, C., Alvarado, M. J., Reid, J. S., Karl, T., Crounse, J. D., and  
581 Wennberg, P. O.: Emission factors for open and domestic biomass burning for use in atmospheric models,  
582 *Atmos. Chem. Phys.*, 11, 4039-4072, <https://doi.org/10.5194/acp-11-4039-2011>, 2011.

583 Allan, J. D., Jimenez, J. L., Williams, P. I., Alfarra, M. R., Bower, K. N., Jayne, J. T., Coe, H., and  
584 Worsnop, D. R.: Quantitative sampling using an Aerodyne Aerosol Mass Spectrometer 1. Techniques of  
585 data interpretation and error analysis, *J. Geophys. Res.-Atmos*, 108, 4090,  
586 <https://doi.org/10.1029/2002JD002358>, 2003.

587 Andreae, M. O. and Merlet, P.: Emission of trace gases and aerosols from biomass burning, *Global*  
588 *Biogeochem. Cy.*, 15, 955-966, <https://doi.org/10.1029/2000GB001382>, 2001.

589 **Andreae, M. O.: Emission of trace gases and aerosols from biomass burning – an updated assessment,**  
590 ***Atmos. Chem. Phys.*, 19, 8523-8546, <https://doi.org/10.5194/acp-19-8523-2019>, 2019. Biomass burning**  
591 **emission factors [https://edmond.mpdl.mpg.de/imeji/collection/op2vVE8m0us\\_gcGC](https://edmond.mpdl.mpg.de/imeji/collection/op2vVE8m0us_gcGC), ver 14 Apr 2021.**

592 Baray, S., Darlington, A., Gordon, M., Hayden, K. L., Leithead, A., Li, S. M., Liu, P. S. K., Mittermeier,  
593 R. L., Moussa, S. G., O'Brien, J., Staebler, R., Wolde, M., Worthy, D., and McLaren, R.: Quantification  
594 of methane sources in the Athabasca Oil Sands Region of Alberta by aircraft mass balance, *Atmos. Chem.*  
595 *Phys.*, 18, 7361-7378, <https://doi.org/10.5194/acp-18-7361-2018>, 2018.

596 Baumgardner, D., Kok, G., and Raga, G.: Warming of the Arctic lower stratosphere by light absorbing  
597 particles, *Geophys. Res. Lett.*, 31, L06117, <https://doi.org/10.1029/2003GL018883>, 2004.

598 Bertschi, I., Yokelson, R. J., Ward, D. E., Babbitt, R. E., Susott, R. A., Goode, J. G., and Hao, W. M.:  
599 Trace gas and particle emissions from fires in large diameter and belowground biomass fuels, *J. Geophys.*  
600 *Res.-Atmos*, 108, 8472, <https://doi.org/10.1029/2002JD002100>, 2003.

601 Cai, Y., Montague, D. C., Mooiweer-Bryan, W., and Deshler, T.: Performance characteristics of the ultra  
602 high sensitivity aerosol spectrometer for particles between 55 and 800nm: Laboratory and field studies, *J.*  
603 *Aerosol Sci.*, 39, 759-769, <https://doi.org/10.1016/j.jaerosci.2008.04.007>, 2008.

604 Clyne, M. A. A., Thrush, B. A., and Wayne, R. P.: Kinetics of the chemiluminescent reaction between  
605 nitric oxide and ozone, *Trans. Faraday Soc.*, 60, 359-370, <https://doi.org/10.1039/TF9646000359>, 1964.

606 Cole, A. S., Steffen, A., Eckley, C. S., Narayan, J., Pilote, M., Tordon, R., Graydon, J. A., St. Louis, V.  
607 L., Xu, X., and Branfireun, B. A.: A survey of mercury in air and precipitation across Canada: Patterns  
608 and trends, *Atmosphere*, 5, 635-668, <https://doi.org/10.3390/atmos5030635>, 2014.

609 DeCarlo, P. F., Dunlea, E. J., Kimmel, J. R., Aiken, A. C., Sueper, D., Crounse, J., Wennberg, P. O.,  
610 Emmons, L., Shinozuka, Y., Clarke, A., Zhou, J., Tomlinson, J., Collins, D. R., Knapp, D., Weinheimer,  
611 A. J., Montzka, D. D., Campos, T., and Jimenez, J. L.: Fast airborne aerosol size and chemistry  
612 measurements above Mexico City and Central Mexico during the MILAGRO campaign, *Atmos. Chem.*  
613 *Phys.*, 8, 4027-4048, <https://doi.org/10.5194/acp-8-4027-2008>, 2008.

614 Ditto, J. C., He, M., Hass-Mitchell, T. N., Moussa, S. G., Hayden, K., Li, S. M., Liggio, J., Leithead, A.,  
615 Lee, P., Wheeler, M. J., Wentzell, J. J. B., and Gentner, D. R.: Atmospheric evolution of emissions from a

616 boreal forest fire: the formation of highly functionalized oxygen-, nitrogen-, and sulfur-containing organic  
617 compounds, *Atmos. Chem. Phys.*, 21, 255-267, <https://doi.org/10.5194/acp-21-255-2021>, 2021.

618 Drewnick, F., Schwab, J. J., Jayne, J. T., Canagaratna, M., Worsnop, D. R., and Demerjian, K. L.:  
619 Measurement of ambient aerosol composition during the PMTACS-NY 2001 using an aerosol mass  
620 spectrometer. Part I: Mass concentrations special issue of aerosol science and technology on findings  
621 from the Fine Particulate Matter Supersites Program, *Aerosol Sci. Tech.*, 38, 92-103,  
622 <https://doi.org/10.1080/02786820390229507>, 2004.

623 Dunlea, E. J., DeCarlo, P. F., Aiken, A. C., Kimmel, J. R., Peltier, R. E., Weber, R. J., Tomlinson, J.,  
624 Collins, D. R., Shinzuka, Y., McNaughton, C. S., Howell, S. G., Clarke, A. D., Emmons, L. K., Apel, E.  
625 C., Pfister, G. G., van Donkelaar, A., Martin, R. V., Millet, D. B., Heald, C. L., and Jimenez, J. L.:  
626 Evolution of Asian aerosols during transpacific transport in INTEX-B, *Atmos. Chem. Phys.*, 9, 7257-  
627 7287, <https://doi.org/10.5194/acp-9-7257-2009>, 2009.

628 Fehsenfeld, F. C., Dickerson, R. R., Hübler, G., Luke, W. T., Nunnermacker, L. J., Williams, E. J.,  
629 Roberts, J. M., Calvert, J. G., Curran, C. M., Delany, A. C., Eubank, C. S., Fahey, D. W., Fried, A.,  
630 Gandrud, B. W., Langford, A. O., Murphy, P. C., Norton, R. B., Pickering, K. E., and Ridley, B. A.: A  
631 ground-based intercomparison of NO, NO<sub>x</sub>, and NO<sub>y</sub> measurement techniques, *J. Geophys. Res.-Atmos.*,  
632 92, 14710-14722, <https://doi.org/10.1029/JD092iD12p14710>, 1987.

633 Gordon, M., Li, S. M., Staebler, R., Darlington, A., Hayden, K., O'Brien, J., and Wolde, M.: Determining  
634 air pollutant emission rates based on mass balance using airborne measurement data over the Alberta oil  
635 sands operations, *Atmos. Meas. Tech.*, 8, 3745-3765, <https://doi.org/10.5194/amt-8-3745-2015>, 2015.  
636

637 Hatch, L. E., Yokelson, R. J., Stockwell, C. E., Veres, P. R., Simpson, I. J., Blake, D. R., Orlando, J. J.,  
638 and Barsanti, K. C.: Multi-instrument comparison and compilation of non-methane organic gas emissions  
639 from biomass burning and implications for smoke-derived secondary organic aerosol precursors, *Atmos.*  
640 *Chem. Phys.*, 17, 1471-1489, <https://doi.org/10.5194/acp-17-1471-2017>, 2017.

641 Hayden, K.L., Li, S.M. Makar, P., Liggio, J., Moussa, S.G., Akingunola, A., McLaren, R., Staebler, R.M.,  
642 Darlington, A., O'Brien, J., Zhang, J., Wolde, M., and Zhang, L.: New methodology shows short  
643 atmospheric lifetimes of oxidized sulfur and nitrogen due to dry deposition, *Atmos. Chem. Phys.*, 21,  
644 8377-8392, <https://doi.org/10.5194/acp-21-8377-2021>, 2021.

645 Jimenez, J. L., Jayne, J. T., Shi, Q., Kolb, C. E., Worsnop, D. R., Yourshaw, I., Seinfeld, J. H., Flagan, R.  
646 C., Zhang, X., Smith, K. A., Morris, J. W., and Davidovits, P.: Ambient aerosol sampling using the  
647 Aerodyne Aerosol Mass Spectrometer, *J. Geophys. Res.-Atmos.*, 108, 8425,  
648 <https://doi.org/10.1029/2001JD001213>, 2003.

649 Khare, P., Marcotte, A., Sheu, R., Walsh, A. N., Ditto, J. C., and Gentner, D. R.: Advances in offline  
650 approaches for trace measurements of complex organic compound mixtures via soft ionization and high-  
651 resolution tandem mass spectrometry, *J. Chromatogr. A*, 1598, 163-  
652 174, <https://doi.org/10.1016/j.chroma.2019.03.037>, 2019.

653 Kleinman, L. I., Springston, S. R., Daum, P. H., Lee, Y. N., Nunnermacker, L. J., Senum, G. I., Wang, J.,  
654 Weinstein-Lloyd, J., Alexander, M. L., Hubbe, J., Ortega, J., Canagaratna, M. R., and Jayne, J.: The time  
655 evolution of aerosol composition over the Mexico City plateau, *Atmos. Chem. Phys.*, 8, 1559-1575,  
656 <https://doi.org/10.5194/acp-8-1559-2008>, 2008.

657 Koss, A. R., Sekimoto, K., Gilman, J. B., Selimovic, V., Coggon, M. M., Zarzana, K. J., Yuan, B.,  
658 Lerner, B. M., Brown, S. S., Jimenez, J. L., Krechmer, J., Roberts, J. M., Warneke, C., Yokelson, R. J.,  
659 and de Gouw, J.: Non-methane organic gas emissions from biomass burning: identification,  
660 quantification, and emission factors from PTR-ToF during the FIREX 2016 laboratory experiment,  
661 *Atmos. Chem. Phys.*, 18, 3299-3319, <https://doi.org/10.5194/acp-18-3299-2018>, 2018.

662 Kupc, A., Williamson, C., Wagner, N. L., Richardson, M., and Brock, C. A.: Modification, calibration,  
663 and performance of the Ultra-High Sensitivity Aerosol Spectrometer for particle size distribution and  
664 volatility measurements during the Atmospheric Tomography Mission (ATom) airborne campaign,  
665 *Atmos. Meas. Tech.*, 11, 369-383, <https://doi.org/10.5194/amt-11-369-2018>, 2018.

666 Lee, B. H., Lopez-Hilfiker, F. D., Mohr, C., Kurtén, T., Worsnop, D. R., and Thornton, J. A.: An Iodide-  
667 Adduct High-Resolution Time-of-Flight Chemical-Ionization Mass Spectrometer: Application to  
668 Atmospheric Inorganic and Organic Compounds, *Environmental Science & Technology*, 48, 6309-6317,  
669 [10.1021/es500362a](https://doi.org/10.1021/es500362a), 2014.

670 Lee, B. H., Lopez-Hilfiker, F. D., Veres, P. R., McDuffie, E. E., Fibiger, D. L., Sparks, T. L., Ebben, C.  
671 J., Green, J. R., Schroder, J. C., Campuzano-Jost, P., Iyer, S., D'Ambro, E. L., Schobesberger, S., Brown,  
672 S. S., Wooldridge, P. J., Cohen, R. C., Fiddler, M. N., Bililign, S., Jimenez, J. L., Kurtén, T., Weinheimer,  
673 A. J., Jaegle, L., and Thornton, J. A.: Flight Deployment of a High-Resolution Time-of-Flight Chemical  
674 Ionization Mass Spectrometer: Observations of Reactive Halogen and Nitrogen Oxide Species, *Journal of*  
675 *Geophysical Research: Atmospheres*, 123, 7670-7686, <https://doi.org/10.1029/2017JD028082>, 2018.

676 Leifer, I., Melton, C. Tratt, D.M., Buckland, K.N., Clarisse, L., Coheur, P., Frash, J., Gupta, M., Johnson,  
677 P.D., Leen, J.B., Van Damme, M., Whitburn, S., and Yurganov, L.: Remote sensing and in situ  
678 measurements of methane and ammonia emissions from a megacity dairy complex: Chino, CA, *Environ.*  
679 *Poll.*, 221, 37-51, <https://doi.org/10.1016/j.envpol.2016.09.083>, 2017.

680 Lerner, B. M., Gilman, J. B., Aikin, K. C., Atlas, E. L., Goldan, P. D., Graus, M., Hendershot, R.,  
681 Isaacman-VanWertz, G. A., Koss, A., Kuster, W. C., Lueb, R. A., McLaughlin, R. J., Peischl, J., Sueper,  
682 D., Ryerson, T. B., Tokarek, T. W., Warneke, C., Yuan, B., and de Gouw, J. A.: An improved, automated  
683 whole air sampler and gas chromatography mass spectrometry analysis system for volatile organic  
684 compounds in the atmosphere, *Atmos. Meas. Tech.*, 10, 291-313, [https://doi.org/10.5194/amt-10-291-](https://doi.org/10.5194/amt-10-291-2017)  
685 [2017](https://doi.org/10.5194/amt-10-291-2017), 2017.

686 Li, S.-M., Leithead, A., Moussa, S. G., Liggio, J., Moran, M. D., Wang, D., Hayden, K., Darlington, A.,  
687 Gordon, M., Staebler, R., Makar, P. A., Stroud, C. A., McLaren, R., Liu, P. S. K., O'Brien, J.,  
688 Mittermeier, R. L., Zhang, J., Marson, G., Cober, S. G., Wolde, M., and Wentzell, J. J. B.: Differences  
689 between measured and reported volatile organic compound emissions from oil sands facilities in Alberta,  
690 *Canada, P. Natl. Acad. Sci. USA*, 114, E3756-E3765, <https://doi.org/10.1073/pnas.1617862114>, 2017.

691 Li, K., Liggio, J., Han, C., Liu, Q., Moussa, S. G., Lee, P., and Li, S.-M.: Understanding the impact of  
692 high-NO<sub>x</sub> conditions on the formation of secondary organic aerosol in the photooxidation of oil sand-  
693 related precursors, *Environ. Sci. Technol.*, 53, 14420-14429, <https://doi.org/10.1021/acs.est.9b05404>,  
694 2019.

695  
696 Li, K., Wentzell, J. J. B., Liu, Q., Leithead, A., Moussa, S. G., Wheeler, M. J., Han, C., Lee, P., Li, S.-M.,  
697 and Liggio, J.: Evolution of atmospheric total organic carbon from petrochemical mixtures, *Environ. Sci.*  
698 *Technol.*, 55, 12841-12851, <https://doi.org/10.1021/acs.est.1c02620>, 2021.

699

700 Liggio, J., Stroud, C. A., Wentzell, J. J. B., Zhang, J., Sommers, J., Darlington, A., Liu, P. S. K., Moussa,  
701 S. G., Leithead, A., Hayden, K., Mittermeier, R. L., Staebler, R., Wolde, M., and Li, S.-M.: Quantifying  
702 the Primary Emissions and Photochemical Formation of Isocyanic Acid Downwind of Oil Sands  
703 Operations, *Environmental Science & Technology*, 51, 14462-14471, 10.1021/acs.est.7b04346, 2017.

704 McGee, T.K.: Evacuating First Nations during wildfires in Canada, *Fire Safety Journ.*, 120,  
705 <https://doi.org/10.1016/j.firesaf.2020.103120>, 2020.

706 McLagan, D. S., Stupple, G. W., Darlington, A., Hayden, K., and Steffen, A.: Where there is smoke there  
707 is mercury: Assessing boreal forest fire mercury emissions using aircraft and highlighting uncertainties  
708 associated with upscaling emissions estimates, *Atmos. Chem. Phys.*, 21, 5635-5653,  
709 <https://doi.org/10.5194/acp-21-5635-2021>, 2021.

710 Middlebrook, A. M., Bahreini, R., Jimenez, J. L., and Canagaratna, M. R.: Evaluation of composition-  
711 dependent collection efficiencies for the aerodyne aerosol mass spectrometer using field data, *Aerosol*  
712 *Sci. Tech.*, 46, 258-271, <https://doi.org/10.1080/02786826.2011.620041>, 2012.

713 Mungall, E. L., Abbatt, J. P. D., Wentzell, J. J. B., Lee, A. K. Y., Thomas, J. L., Blais, M., Gosselin, M.,  
714 Miller, L. A., Papakyriakou, T., Willis, M. D., and Liggio, J.: Microlayer source of oxygenated volatile  
715 organic compounds in the summertime marine Arctic boundary layer, *Proceedings of the National*  
716 *Academy of Sciences of the United States of America*, 114, 6203-6208, 10.1073/pnas.1620571114, 2017.

717 Neuman, J. A., Huey, L. G., Ryerson, T. B., and Fahey, D. W.: Study of Inlet Materials for Sampling  
718 Atmospheric Nitric Acid, *Environmental Science & Technology*, 33, 1133-1136, 10.1021/es980767f,  
719 1999.

720 Penkett, S., Gilge, S., Plass-Duelmer, C., Galbally, I., Brough, N., Bottenheim, J., Flocke, F., Gerwig, H.,  
721 Lee, J., Milton, M., Rohrer, F., Ryerson, T., Steinbacher, M., Torseth, K., and Wielgosz, R.: WMO/GAW  
722 expert workshop on global long-term measurements of nitrogen oxides and recommendations for GAW  
723 nitrogen oxides network, World Meteorological Organization, Hohenpeissenberg, Germany, 2011.  
724

725 Permar, W., Wang, Q., Selimovic, V., Wielgasz, C., Yokelson, R. J., Hornbrook, R. S., Hills, A. J., Apel,  
726 E. C., Ku, I.-T., Zhou, Y., Sive, B. C., Sullivan, A. P., Collett Jr, J. L., Campos, T. L., Palm, B. B., Peng,  
727 Q., Thornton, J. A., Garofalo, L. A., Farmer, D. K., Kreidenweis, S. M., Levin, E. J. T., DeMott, P. J.,  
728 Flocke, F., Fischer, E. V., and Hu, L.: Emissions of trace organic gases from western U.S. wildfires based  
729 on WE-CAN aircraft measurements, *J. Geophys. Res.-Atmos*, 126, e2020JD033838,  
730 <https://doi.org/10.1029/2020JD033838>, 2021.

731 Quinn, P. K., Bates, T. S., Coffman, D., Onasch, T. B., Worsnop, D., Baynard, T., de Gouw, J. A.,  
732 Goldan, P. D., Kuster, W. C., Williams, E., Roberts, J. M., Lerner, B., Stohl, A., Pettersson, A., and  
733 Lovejoy, E. R.: Impacts of sources and aging on submicrometer aerosol properties in the marine boundary  
734 layer across the Gulf of Maine, *J. Geophys. Res.-Atmos*, 111, D23S36,  
735 <https://doi.org/10.1029/2006JD007582>, 2006.

736 Reid, J. S., and Hobbs, P. V.: Physical and optical properties of young smoke from individual biomass  
737 fires in Brazil, *J. Geophys. Res.-Atmos.*, 103, 32013-32030, 10.1029/98jd00159, 1998.

738 Reid, J. S., Koppmann, R., Eck, T. F., and Eleuterio, D. P.: A review of biomass burning emissions part  
739 II: intensive physical properties of biomass burning particles, *Atmos. Chem. Phys.*, 5, 799-825,  
740 10.5194/acp-5-799-2005, 2005.

741 Ridley, B. A. and Grahek, F. E.: A small, low flow, high sensitivity reaction vessel for NO  
742 chemiluminescence detectors, *J. Atmos. Ocean. Tech.*, 7, 307-311, [https://doi.org/10.1175/1520-](https://doi.org/10.1175/1520-0426(1990)007<0307:Aslfhs>2.0.Co;2)  
743 [0426\(1990\)007<0307:Aslfhs>2.0.Co;2](https://doi.org/10.1175/1520-0426(1990)007<0307:Aslfhs>2.0.Co;2), 1990.

744 Roberts, J. M., Veres, P., Warneke, C., Neuman, J. A., Washenfelder, R. A., Brown, S. S., Baasandorj,  
745 M., Burkholder, J. B., Burling, I. R., Johnson, T. J., Yokelson, R. J., and De Gouw, J.: Measurement of  
746 HONO, HNCO, and other inorganic acids by negative-ion proton-transfer chemical-ionization mass  
747 spectrometry (NI-PT-CIMS): Application to biomass burning emissions, *Atmospheric Measurement*  
748 *Techniques*, 3, 981-990, 10.5194/amt-3-981-2010.

749 Schwarz, J. P., Gao, R. S., Fahey, D. W., Thomson, D. S., Watts, L. A., Wilson, J. C., Reeves, J. M.,  
750 Darbeheshti, M., Baumgardner, D. G., Kok, G. L., Chung, S. H., Schulz, M., Hendricks, J., Lauer, A.,  
751 Kärcher, B., Slowik, J. G., Rosenlof, K. H., Thompson, T. L., Langford, A. O., Loewenstein, M., and  
752 Aikin, K. C.: Single-particle measurements of midlatitude black carbon and light-scattering aerosols from  
753 the boundary layer to the lower stratosphere, *J. Geophys. Res.-Atmos*, 111, D16207,  
754 <https://doi.org/10.1029/2006JD007076>, 2006.

755 Sekimoto, K., Li, S.-M., Yuan, B., Koss, A., Coggon, M., Warneke, C., and de Gouw, J.: Calculation of  
756 the sensitivity of proton-transfer-reaction mass spectrometry (PTR-MS) for organic trace gases using  
757 molecular properties, *Int. J. Mass Spectrom.*, 421, 71-94, <https://doi.org/10.1016/j.ijms.2017.04.006>,  
758 2017.

759 Selimovic, V., Yokelson, R. J., McMeeking, G. R., and Coefield, S.: In situ measurements of trace gases,  
760 PM, and aerosol optical properties during the 2017 NW US wildfire smoke event, *Atmos. Chem. Phys.*,  
761 19, 3905-3926, <https://doi.org/10.5194/acp-19-3905-2019>, 2019.

762 Sheu, R., Marcotte, A., Khare, P., Charan, S., Ditto, J. C., and Gentner, D. R.: Advances in offline  
763 approaches for chemically speciated measurements of trace gas-phase organic compounds via adsorbent  
764 tubes in an integrated sampling-to-analysis system, *J. Chromatogr. A*, 1575, 80-  
765 90, <https://doi.org/10.1016/j.chroma.2018.09.014>, 2018.

766 Stecher III, H. A., Luther III, G. W., MacTaggart, D. L., Farwell, S. O., Crosley, D. R., Dorko, W. D.,  
767 Goldan, P. D., Beltz, N., Krischke, U., Luke, W. T., Thornton, D. C., Talbot, R. W., Lefer, B. L., Scheuer,  
768 E. M., Benner, R. L., Wu, J., Saltzman, E. S., Gallagher, M. S., and Ferek, R. J.: Results of the Gas-Phase  
769 Sulfur Intercomparison Experiment (GASIE): Overview of experimental setup, results and general  
770 conclusions, *J. Geophys. Res.-Atmos*, 102, 16219-16236, <https://doi.org/10.1029/97JD01362>, 1997.

771 Stephens, M., Turner, N., and Sandberg, J.: Particle identification by laser-induced incandescence in a  
772 solid-state laser cavity, *Appl. Optics*, 42, 3726-3736, <https://doi.org/10.1364/ao.42.003726>, 2003.

773 Stockwell, C. E., Kupc, A., Witkowski, B., Talukdar, R. K., Liu, Y., Selimovic, V., Zarzana, K. J.,  
774 Sekimoto, K., Warneke, C., Washenfelder, R. A., Yokelson, R. J., Middlebrook, A. M., and Roberts, J.  
775 M.: Characterization of a catalyst-based conversion technique to measure total particulate nitrogen and  
776 organic carbon and comparison to a particle mass measurement instrument, *Atmos. Meas. Tech.*, 11,  
777 2749-2768, 10.5194/amt-11-2749-2018, 2018.

778 Veres, P. R., and Roberts, J. M.: Development of a photochemical source for the production and  
779 calibration of acyl peroxy compounds, *Atmos. Meas. Tech.*, 8, 2225-2231, 10.5194/amt-8-2225-  
780 2015, 2015.

781 Veres, P., Roberts, J. M., Burling, I. R., Warneke, C., de Gouw, J., and Yokelson, R. J.: Measurements of  
782 gas-phase inorganic and organic acids from biomass fires by negative-ion proton-transfer chemical-

783 ionization mass spectrometry, *J. Geophys. Res.-Atmos*, 115, D23302,  
784 <https://doi.org/10.1029/2010JD014033>, 2010.

785 Ward, D. E. and Radke, L. F.: Emissions measurements from vegetation fires: A comparative evaluation  
786 of methods and results, in: *Fire in the Environment: The Ecological, Atmospheric, and Climatic*  
787 *Importance of Vegetation Fires*. Dahlem Workshop Reports: Environmental Sciences Research Report  
788 13, edited by: Crutzen, P. J., and Goldammer, J. G., John Wiley & Sons, Chichester, England, 53-76,  
789 1993.

790 Williams, E. J., Baumann, K., Roberts, J. M., Bertman, S. B., Norton, R. B., Fehsenfeld, F. C.,  
791 Springston, S. R., Nunnermacker, L. J., Newman, L., Olszyna, K., Meagher, J., Hartsell, B., Edgerton, E.,  
792 Pearson, J. R., and Rodgers, M. O.: Intercomparison of ground-based NO<sub>y</sub> measurement techniques, *J.*  
793 *Geophys. Res.-Atmos*, 103, 22261-22280, <https://doi.org/10.1029/98JD00074>, 1998.

794

795

796

797